Honors Undergraduate Thesis

Design and Experimental Study of a Mechanical System with Air Springs

Submitted to the

Engineering Honors Committee
As partial requirement for graduation with distinction
in the Department of Mechanical Engineering

119 Hitchcock Hall
College of Engineering
The Ohio State University
Columbus, Ohio 43210

By

Benjamin Barszcz

Department of Mechanical Engineering
Columbus, Ohio 43210

Advisor: Prof. R. Singh

November 21, 2008

Contents

List of variables

$y(t)$	Vertical (translational) displacement of beam (m)
$\theta(t)$	Rotation of beam about horizontal through location of y (rad)
$\omega_{n,1}$	Natural frequency corresponding to first mode (rad/s)
$\omega_{n,2}$	Natural frequency corresponding to second mode (rad/s)
m	Mass of beam = 55.7 kg = 122.54 lb_m
ζ	Damping ratio of system (at a given mode)
k_1	Stiffness of air spring at proximal end of beam (N/m)
k_2	Stiffness of air spring at distal end of beam (N/m)
c_1	Viscous damping coefficient at proximal end of beam [(N-s)/m]
c_2	Viscous damping coefficient at distal end of beam [(N-s)/m]
l_1	Distance from k_1 to center of gravity of beam = 0.498475 m = 21.625 in
l_2	Distance from k_2 to center of gravity of beam = 0.498475 m = 21.625 in
L	Span length of beam = $l_1 + l_2$ = 0.99695 m = 43.25 in
l_3	Distance from k_1 to geometric center of beam = 0.498475 m = 21.625 in
l_4	Distance from k_1 to geometric center of beam = 0.498475 m = 21.625 in
e	Eccentricity y (from geometric center to center of gravity) = 0 m
J	Mass moment of inertia about center of gravity of beam (kg-m^2)
F(t)	Excitation (dynamic) force
a	Magnitude of excitation force = 1 N (for impulse excitation)
s_1	Torque arm from impulse excitation to center of gravity = 0.534 m = 21.378 in
$y_1(t)$	Reference translational displacement (m)
l_g	Distance from reference displacement to center of gravity of beam (m)
d_1	Distance from k_1 to location of reference displacement (m)
η	Span length of beam from reference displacement to arbitrary displacement (m)
$y_x(t)$	Arbitrary translational displacement with respect to reference y_1 (m)
[v]	Modal vector from eigensolution
[m]	Normalized modal vector
[M]	Mass (inertia) matrix
[K]	Stiffness matrix
λ[I]	Eigenvalue matrix (undamped natural frequencies)
ω_d	Damped/experimental natural frequency (rad/s)
H	Transfer function, y/F in Laplace or frequency domain
a(t)	Acceleration measurement of beam from accelerometer (m/s^2)
$y_{1,}\omega_{n,x}$	Amplitude of reference displacement (at a given mode)
$y_{x,}\omega_{n,x}$	Amplitude of arbitrary displacement with respect to reference displacement (at a given mode)
$A_{1,}\omega_{n,x}$	Amplitude of imaginary part of accelerance at location 1 (at a given mode) [(m/s^2)/N]
$A_{2,x}$	Amplitude of imaginary part of accelerance at location 2 (at a given mode) [(m/s^2)/N]
S/N	Signal to noise ratio; quantity of coherence of the measurement system
$\overline{\omega_d}$	Average of damped/experimental natural frequencies measured at all locations for a given pressure (rad/s)
[C]	Viscous damping matrix

Abstract

A laboratory system consisting of a rigid beam and two air springs system has been designed and constructed; this system simulates the planar dynamics of an automobile suspension. The dynamic response of this system was investigated with respect to two natural frequencies ($\omega_{n,1}$ and $\omega_{n,2}$), damping ratios and vibration modes in order to better understand the physics of such systems. It has been seen through experimental that nonlinear behavior is negligible for small displacements. Accordingly, this system can be, and is modeled linearly for small motions.

For a certain range of displacements, the system parameters and modal properties have been characterized and accurately determined. A transfer function model has been developed which can be used to successfully predict and approximate frequency responses. Experimentally, this system is primarily described by a translational mode at $\omega_{n,1}$ and a rotational mode at $\omega_{n,2}$. Future work should focus on the nonlinear dynamics of the system.

1 - Background & Literature Review

In many real-life mechanical systems, significant nonlinearities are readily present in functions describing stiffness *k* and damping *c elements*. Geared systems, transmissions, suspensions and clutches are common examples of mechanical systems where this behavior can be observed [1]. Knowledge and integration of these nonlinearities analytically is useful for design purposes, especially since such properties are encountered in systems both intentionally and unintentionally in engineering practice [1-7].

Nonlinear spring elements are very important and useful tools in the mechanical world, especially in the automotive discipline. Elements such as coil springs, c-springs, leaf springs, and rubber stoppers are utilized in systems ranging from suspensions to passenger seats. Of particular interest is the air spring nonlinear stiffness element, which is typically soft with respect to other mechanical spring elements in automobiles. As a result, air springs introduce lower natural frequencies [2].

Nonlinearities can cause difficulties in analytical investigations. However, the linearized behavior of nonlinear systems must be first examined. This is the main goal of this study, where a two degree of freedom system is experimentally and analytically evaluated.

2 - Objectives

- Design, build, and test an experiment exhibiting:
    - Dynamic behavior comparable to that of an automobile suspension
    - Low natural frequency
    - A limit of two modes
    - Nonlinearities with respect to stiffness
- Verify the presence of nonlinearity (if any)
- Determine the system parameters (ω_n and ζ) over small displacements
- Investigate the mode shapes of experiment
- Develop an analytical model to describe the dynamics of the experiment

3 - Design of Experiment

3.1 – Linear Theory

The experimental apparatus was designed using linear theory to exhibit the dynamic behavior of a car suspension. The primary tool for investigating the relationship between the input and output of a linear system is the transfer function. The transfer function of a mechanical system describes the behavior of the system based on its physical parameters and the relationship between input and output. The behavior of linear systems do not depend on the input or output, so the transfer function can be expressed as a ratio of the input and output during a steady-state

condition. In order to describe a system with a transfer function, the physical parameters of the system must be linear in nature. Conventionally, a system can be completely described by mass, damping and stiffness parameters with a second order, linear time-invariant ordinary differential equation. Assuming a continuous and differentiable displacement *y(t)* over its finite domain, this differential equation will look as follows:

$$\begin{aligned} m\frac{d^2y}{dt^2} + c\frac{dy}{dt} + ky(t) &= aF(t) \\ \frac{d^2y}{dt^2} + 2\zeta\omega_n\frac{dy}{dt} + \omega_n{}^2 y(t) &= \frac{aF(t)}{m} \end{aligned} \qquad (1)$$

The two above equations are equivalent. The first is expressed in units of force, whereas normalizing by the system mass changes this to units of acceleration. Since the displacement is continuous, *y(t)* can be transformed from the time domain and investigated in Laplace space and the frequency domain using the Laplace Transform. Taking the Laplace Transform of *y(t),* the differential equation of (1) becomes:

$$\begin{aligned} &m[s^2Y(s) - sy(t=0) - v(t=0)] + c[sY(s) - y(t=0)] + kY(s) = aF(s) \\ &[s^2Y(s) - sy(t=0) - v(t=0)] + 2\zeta\omega_n[sY(s) - y(t=0)] + \omega_n{}^2Y(s) = \frac{aF(s)}{m} \end{aligned} \qquad (2)$$

When the system starts at rest and in its equilibrium position, the initial velocity and displacement conditions of the system will evaluate to zero, and the equation can be expressed as so:

$$\begin{aligned} Y(s)[ms^2 + cs + k] &= aF(s) \\ Y(s)[s^2 + 2\zeta\omega_n s + \omega_n{}^2] &= \frac{aF(s)}{m} \end{aligned} \qquad (3)$$

The transfer function of this system is thus expressed as the ratio of the system output displacement response over the input force as follows:

$$\begin{aligned} \frac{Y(s)}{F(s)} = H(s) &= \frac{a}{[ms^2 + cs + k]} \\ \frac{Y(s)}{F(s)} = H(s) &= \frac{a/m}{[s^2 + 2\zeta\omega_n s + \omega_n{}^2]} \end{aligned} \qquad (4)$$

This transfer function in the frequency domain has the following form, where s = jω:

$$\frac{Y(j\omega)}{F(j\omega)} = H(j\omega) = \frac{a}{[m(j\omega)^2 + c(j\omega) + k]}$$
$$\frac{Y(j\omega)}{F(j\omega)} = H(j\omega) = \frac{a/m}{[(j\omega)^2 + 2\zeta\omega_n(j\omega) + \omega_n^{\,2}]} \quad (5)$$

The above transfer function is called the frequency response of the system. The frequency response can be used to find the magnitude ratio of the output to the input, in addition to their phase angle over all frequencies. This is useful for determining the natural frequencies of the system, which are located at the system's resonant frequencies.

3.2 – 2-DOF Analytical Model

Applying the results of transfer function methodology for linear analysis, it is possible to investigate the output of a given system with respect to some known excitation input. Several well-accepted models for automobile dynamic suspension behavior apply to two-dimensional responses involving a linear displacement and rotational degree of freedom, which are described by second order differential equations and transfer functions for small displacement ranges. A schematic of such models is depicted below in Figure 1.

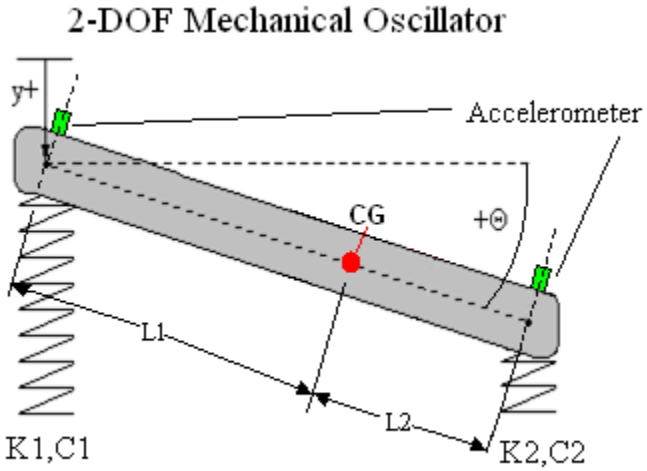

Figure 1 – Schematic of two-dimensional dynamic model

The system is modeled as a beam-mass. It is influenced by stiffness and damping elements at its ends, where it is coupled to the reference frame of the ground. The system's motion is described by a mode of linear translation in the vertical direction, along with a mode of rotation defined with respect to the horizontal from the location of displacement. Depending on the choice of the coordinate system (specifically, the location of the displacement), coordinate coupling of these modes will occur in different manners. The condition of static coupling exists when the linear displacement of the system is taken at the center of mass of the beam. This condition is defined

by a non-diagonal system stiffness matrix and a diagonal mass matrix, and is described by the following equations of motion [8]:

$$\begin{pmatrix} m & 0 \\ 0 & J \end{pmatrix}\begin{bmatrix} \frac{d^2y}{dt^2} \\ \frac{d^2\theta}{dt^2} \end{bmatrix}+\begin{pmatrix} c_1+c_2 & c_2l_2-c_1l_1 \\ c_2l_2-c_1l_1 & c_1{l_1}^2+c_2{l_2}^2 \end{pmatrix}\begin{bmatrix} \frac{dy}{dt} \\ \frac{d\theta}{dt} \end{bmatrix}+\begin{pmatrix} k_1+k_2 & k_2l_2-k_1l_1 \\ k_2l_2-k_1l_1 & k_1{l_1}^2+k_2{l_2}^2 \end{pmatrix}\begin{bmatrix} y \\ \theta \end{bmatrix}=\begin{bmatrix} aF(t) \\ s_1aF(t) \end{bmatrix} \quad (6)$$

Dynamic coupling of the modes exists when the stiffness matrix is diagonal. This only occurs when the linear displacement of the system is taken at the geometric center of the beam, and the geometric and mass centers do not coincide. By choosing this coordinate coupling, static coupling gets eliminated, i.e., mass matrix is now non-diagonal and the stiffness matrix becomes diagonal. The location of dynamic coupling is commonly referred to as the elastic center of the mass. What is unique about this choice of coordinates is that application of an eccentric normal force at the geometric center causes purely translational motion. Dynamic coupling is expressed by the following equations [8]:

$$\begin{pmatrix} m & me \\ me & J \end{pmatrix}\begin{bmatrix} \frac{d^2y}{dt^2} \\ \frac{d^2\theta}{dt^2} \end{bmatrix}+\begin{pmatrix} c_1+c_2 & 0 \\ 0 & c_1{l_3}^2+c_2{l_4}^2 \end{pmatrix}\begin{bmatrix} \frac{dy}{dt} \\ \frac{d\theta}{dt} \end{bmatrix}+\begin{pmatrix} k_1+k_2 & 0 \\ 0 & k_1{l_3}^2+k_2{l_4}^2 \end{pmatrix}\begin{bmatrix} y \\ \theta \end{bmatrix}=\begin{bmatrix} aF(t) \\ s_1aF(t) \end{bmatrix} \quad (7)$$

Equations (6) and (7) represent special cases for coordinate coupling in this model. In the general case, there exists both static and dynamic coupling in the motion of the beam (both the mass and stiffness matrices are non-diagonal). When the linear displacement is chosen at any other location than the center of gravity or geometry, this will be the case. For the general case, the motions of equation used to describe the system can be defined by starting at the end of the beam and using the kinematic relationship between displacement and rotation. The following equations of motion govern the motion of the system when the location of linear displacement is defined at the end of the beam at location of stiffness element k_1 [8]:

$$\begin{pmatrix} m & ml_1 \\ ml_1 & J \end{pmatrix}\begin{bmatrix} \frac{d^2y}{dt^2} \\ \frac{d^2\theta}{dt^2} \end{bmatrix}+\begin{pmatrix} c_1+c_2 & c_2(l_1+l_2) \\ c_2(l_1+l_2) & c_2(l_1+l_2)^2 \end{pmatrix}\begin{bmatrix} \frac{dy}{dt} \\ \frac{d\theta}{dt} \end{bmatrix}+\begin{pmatrix} k_1+k_2 & k_2(l_1+l_2) \\ k_2(l_1+l_2) & k_2(l_1+l_2)^2 \end{pmatrix}\begin{bmatrix} y \\ \theta \end{bmatrix}=\begin{bmatrix} aF(t) \\ s_1aF(t) \end{bmatrix} \quad (8)$$

For some distance d_1 along the span length of the beam from the end of the beam and spring element K_1, the motion of the system can be transformed as follows:

$$\begin{pmatrix} m & ml_g \\ ml_g & J \end{pmatrix}\begin{bmatrix} \frac{d^2y_1}{dt^2} \\ \frac{d^2\theta}{dt^2} \end{bmatrix}+\begin{pmatrix} c_1+c_2 & c_2(L-d_1)-c_1d_1 \\ c_2(L-d_1)-c_1d_1 & c_1d_1^{\,2}+c_2(L-d_1)^2 \end{pmatrix}\begin{bmatrix} \frac{dy_1}{dt} \\ \frac{d\theta}{dt} \end{bmatrix}+$$
$$\begin{pmatrix} k_1+k_2 & k_2(L-d_1)-k_1d_1 \\ k_2(L-d_1)-k_1d_1 & k_1d_1^{\,2}+k_2(L-d_1)^2 \end{pmatrix}\begin{bmatrix} y_1 \\ \theta \end{bmatrix}=\begin{bmatrix} aF(t) \\ s_1aF(t) \end{bmatrix} \quad (9)$$

By applying this transformation, the system is now two degrees of freedom in *any* location y_1 from the end of the beam and θ. Therefore, (9) can be regarded as the general case of dynamic motion of the beam when one mode is linear displacement, and the other, rotation. It can further be expressed as a pair of transfer functions for each mode by using Laplace transformation as follows:

$$\begin{pmatrix} m & ml_g \\ ml_g & J \end{pmatrix}\begin{bmatrix} s^2Y_1(s) \\ s^2\Theta(s) \end{bmatrix}+\begin{pmatrix} c_1+c_2 & c_2(L-d_1)-c_1d_1 \\ c_2(L-d_1)-c_1d_1 & c_1d_1^{\,2}+c_2(L-d_1)^2 \end{pmatrix}\begin{bmatrix} sY_1(s) \\ s\Theta(s) \end{bmatrix}+$$
$$\begin{pmatrix} k_1+k_2 & k_2(L-d_1)-k_1d_1 \\ k_2(L-d_1)-k_1d_1 & k_1d_1^{\,2}+k_2(L-d_1)^2 \end{pmatrix}\begin{bmatrix} Y_1(s) \\ \Theta(s) \end{bmatrix}=\begin{bmatrix} aF(s) \\ s_1aF(s) \end{bmatrix} \quad (10)$$

Breaking up the coupled system from its matrix formulation to its Y_1 and Θ equations yields the following:

$$\begin{aligned} &Y_1(s)(P)+\Theta(s)(T)=aF(s) \\ &\Theta(s)(R)+Y_1(s)(T)+=as_1F(s) \\ &where: \\ &P=[ms^2+(c_1+c_2)s+(k_1+k_2)] \\ &T=[ml_gs^2+(c_2(L-d_1)-c_1d_1)s+(k_2(L-d_1)-k_1d_1)] \\ &R=[Js^2+(c_1d_1^{\,2}+c_2(L-d_1)^2)s+(k_1d_1^{\,2}+k_2(L-d_1)^2)] \end{aligned} \quad (11)$$

Using the equation of rotation, Θ can be expressed as a function of Y_1 as so:

$$\Theta(s)=\frac{s_1aF(s)-Y_1(s)(T)}{R} \quad (12)$$

The transfer function of the system with respect to linear displacement can be found by solving the system of two equations in unknowns Y_1 and Θ. With knowledge of Θ from the equation of rotation, the transfer function of the system with respect to the displacement mode can be expressed as follows:

$$Y_1(s)(P)+\left[\frac{s_1 aF(s)-Y_1(s)(T)}{R}\right]T=aF(s);$$

$$Y_1(s)[P-\frac{T^2}{R}]=aF(s)[1-\frac{s_1 T}{R}]; \qquad (13)$$

$$\frac{Y_1(s)}{F(s)}=a\left[\frac{1-\frac{s_1 T}{R}}{P-\frac{T^2}{R}}\right]$$

Back-substitution of the above transfer function into the Θ expression in (12) yields the following system transfer function with respect to the rotational mode:

$$\frac{\Theta(s)}{F(s)}=\frac{s_1 a}{R}-\frac{aT}{R}\left[\frac{1-\frac{s_1 T}{R}}{P-\frac{T^2}{R}}\right] \qquad (14)$$

It is useful to express the two degrees of freedom of the system in terms of two linear displacements, especially for mode shape investigation and experimental measurement purposes. The displacement at any distance η from linear displacement y_1 can be found using the following kinematic relation to rotation:

$$y_x = y_1 + \eta\theta \qquad (15)$$

Taking the Laplace Transformation on both sides of (15) and solving for Θ yields the following:

$$\Theta(s)=\frac{Y_x(s)-Y_1(s)}{\eta} \qquad (16)$$

By plugging the above expression for Θ into the Y_1 and Θ equations of equation (11), it is possible to eliminate the rotational mode altogether and couple Y_1 with Y_x. Substituting Θ into both equations yields the following:

$$\begin{aligned} &Y_1(s)(P)+\left[\frac{Y_x(s)-Y_1(s)}{\eta}\right](T)=aF(s) \\ &\left[\frac{Y_x(s)-Y_1(s)}{\eta}\right](R)+Y_1(s)(T)+=as_1F(s) \end{aligned} \qquad (17)$$

In matrix form, (17) can be simplified algebraically as follows:

$$\begin{pmatrix} m-\frac{ml_g}{\eta} & \frac{ml_g}{\eta} \\ ml_g-\frac{J}{\eta} & \frac{J}{\eta} \end{pmatrix}\begin{bmatrix} \frac{d^2y_1}{dt^2} \\ \frac{d^2y_x}{dt^2} \end{bmatrix}+\begin{pmatrix} c_1+c_2-\frac{c_2(L-d_1)-c_1d_1}{\eta} & \frac{c_2(L-d_1)-c_1d_1}{\eta} \\ c_2(L-d_1)-c_1d_1-\frac{c_1d_1^2+c_2(L-d_1)^2}{\eta} & \frac{c_1d_1^2+c_2(L-d_1)^2}{\eta} \end{pmatrix}\begin{bmatrix} \frac{dy_1}{dt} \\ \frac{dy_x}{dt} \end{bmatrix}+$$
$$\begin{pmatrix} k_1+k_2-\frac{k_2(L-d_1)-k_1d_1}{\eta} & \frac{k_2(L-d_1)-k_1d_1}{\eta} \\ k_2(L-d_1)-k_1d_1-\frac{k_1d_1^2+k_2(L-d_1)^2}{\eta} & \frac{k_1d_1^2+k_2(L-d_1)^2}{\eta} \end{pmatrix}\begin{bmatrix} y_1 \\ y_x \end{bmatrix}=\begin{bmatrix} aF(t) \\ s_1aF(t) \end{bmatrix} \quad (18)$$

Solving the system of two equations in two unknowns Y_1 and Y_x in a similar manner to the algebraic operation performed in (13) yields the following transfer function

$$\frac{Y_x(s)}{F(s)}=a\left[\frac{1-\frac{s_1T}{R}}{P-\frac{T^2}{R}}\right]\left[1-\frac{a\eta T}{R}\right]+\frac{a\eta s_1}{R} \quad (19)$$

This is the general expression for the transfer function of the system at *any* location with reference to y_1. In other words, by defining some distance d_1 from the end of the beam and length η along the span of the beam from y_1, an arbitrary transfer function for linear displacement is known. For this reason, (19) can be considered the general case for dynamic motion of the beam when both modes are linear displacements. It was chosen to model the motion of the system due to the flexibility it offered with respect to testing system dynamics for various configurations and setups. In specific, asymmetry could be introduced to the system with respect to both excitation loading as well as end stiffness, if desired. In addition, acceleration measurements could be made anywhere along the span of the beam to describe its mode of displacement.

3.3 – Modal Analysis and the Eigenvalue Formulation

Minimal damping is expected for a beam simply supported by air springs at each of its ends, so the damping matrix is negligible and was assumed to tend to zero for subsequent linear design purposes. Accordingly, the mass of the beam and the required spring stiffness were chosen in a manner so as to yield a desired set of natural frequencies. Namely, the beam and springs were chosen so that the modes of the system approximated the natural frequencies of a typical car suspension, which is of the order of 2-5 Hz. For this reason, air springs were desirable candidates as stiffness members, due to their low stiffness and nonlinear nature. This was difficult to accomplish, as satisfying this criterion for natural frequencies dictated that the mass of the beam be significantly larger than the stiffnesses located at its ends. Designing in this manner constrained the system to small displacements and localized linear behavior when excitation was not large.

The stiffness and mass of the system were determined using a Matlab script, which found all solutions of system equivalent stiffness, (k_1 + k_2) and mass, m, which satisfied this range of natural frequencies. It did so on the premise of Kramer's rule and the Eigenvalue problem for undamped modal analysis, which is the matrix form for the natural frequency solution $\omega_n^2 = [(k_1$

$+ k_2) /m]^2$. Using the mass and stiffness matrices of equations (9) and (18), modal analysis was performed using the following expressions:

$$([M]^{-1}[K]-\lambda[I])[v]=0$$

$$(9)\rightarrow\left[\begin{pmatrix} m & ml_g \\ ml_g & J \end{pmatrix}^{-1}\begin{pmatrix} k_1+k_2 & k_2(L-d_1)-k_1d_1 \\ k_2(L-d_1)-k_1d_1 & k_1d_1^2+k_2(L-d_1)^2 \end{pmatrix}-\begin{pmatrix} \omega_{n,1}{}^2 & 0 \\ 0 & \omega_{n,2}{}^2 \end{pmatrix}\right][v]=0 \tag{20}$$

$$(18)\rightarrow\left[\begin{pmatrix} m-\dfrac{ml_g}{\eta} & \dfrac{ml_g}{\eta} \\ ml_g-\dfrac{J}{\eta} & \dfrac{J}{\eta} \end{pmatrix}^{-1}\begin{pmatrix} k_1+k_2-\dfrac{k_2(L-d_1)-k_1d_1}{\eta} & \dfrac{k_2(L-d_1)-k_1d_1}{\eta} \\ k_2(L-d_1)-k_1d_1-\dfrac{k_1d_1^2+k_2(L-d_1)^2}{\eta} & \dfrac{k_1d_1^2+k_2(L-d_1)^2}{\eta} \end{pmatrix}-\begin{pmatrix} \omega_{n,1}{}^2 & 0 \\ 0 & \omega_{n,2}{}^2 \end{pmatrix}\right][v]=0$$

These equations, although very different in appearance, yield the same exact set of natural frequencies for the system, regardless of the different coordinates. This is due to the fact that natural frequency is a global system parameter in linear systems, and the system of two modal displacements in (18) was determined kinematically from Θ. Accordingly, it was determined that a mass of m = 125.54 lb_f and the stiffness represented by the static load-deflection curve of the 2M2A Firestone air spring were appropriate. The 2M2A is a low-load carrying device that operates at a nominal height of two inches. Figure 2 below displays the 2M2A.

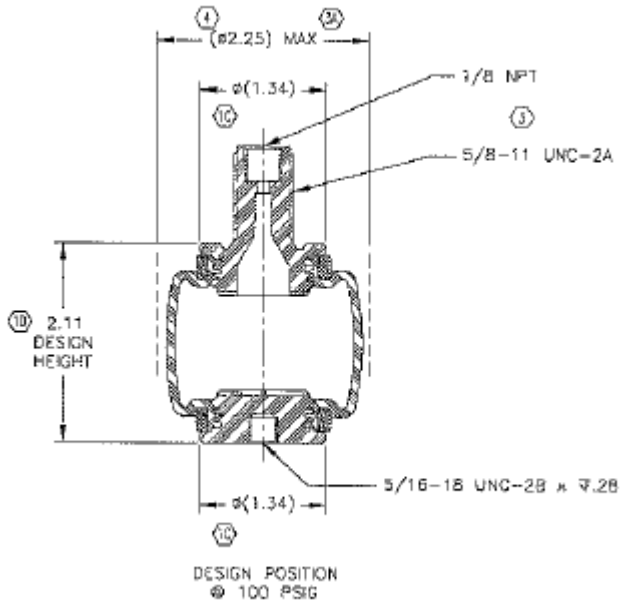

Figure 2 – Engineering drawing of Firestone 2M2A air spring assembly

3.4 – Numerical Simulations

Once again using equations (9) and (18), iterative, linear simulations in Simulink were conducted to determine the geometric and material parameters of the beam. Namely, the geometry and

material of the beam were designed to be sufficiently long so as to satisfy the small angle approximation and previously determined system mass. A 2"x5" hot-rolled steel beam of length 43.25" was seen to perform sufficiently for this purpose. The Simulink diagram pictured below in Figure 3 was used to excite the beam sinusoidally in making these determinations, where the stiffness, damping and mass values could be varied based on the system of equations being considered.

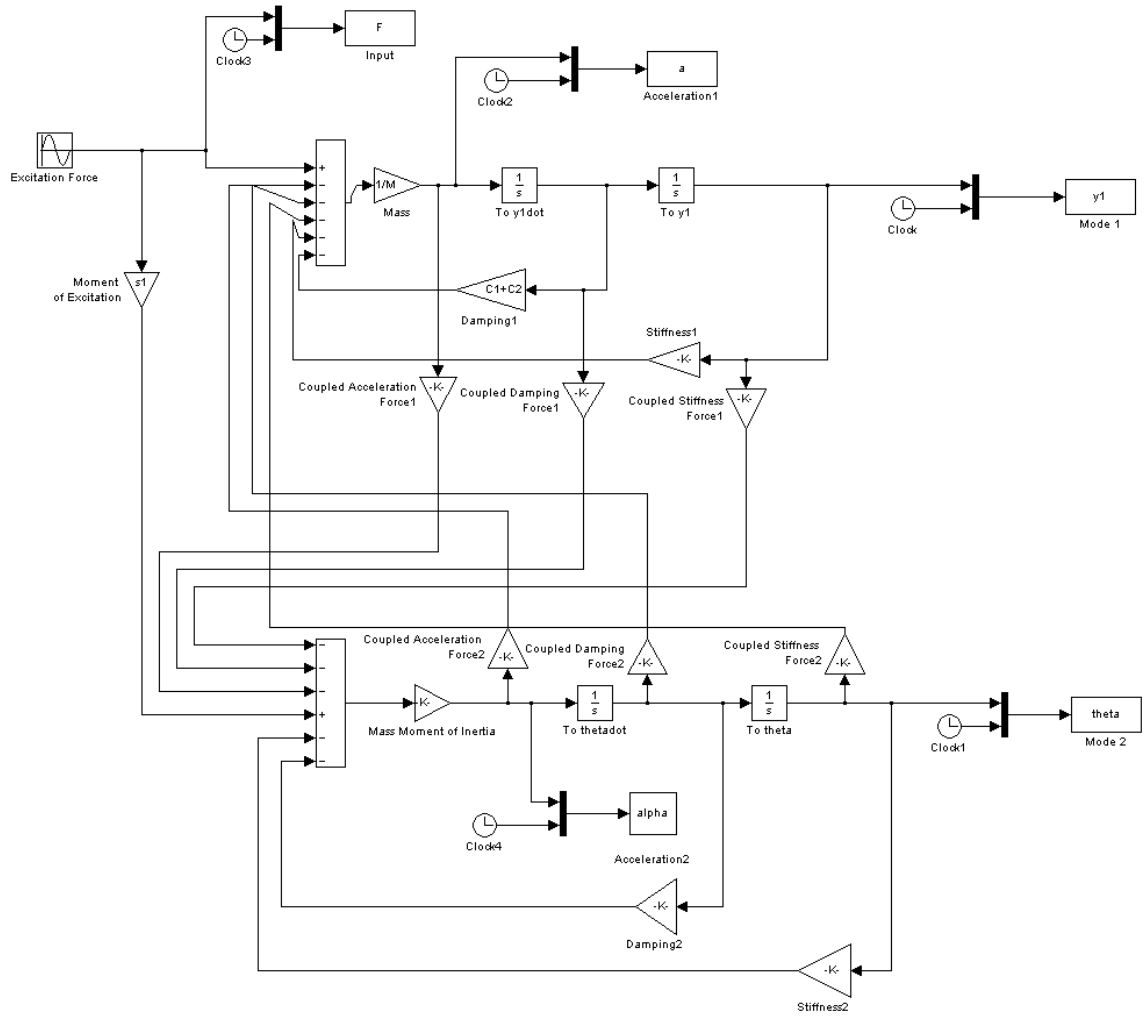

Figure 3 – Simulink numerical model used for geometric sizing, materials determination, and linear simulations of system

3.5 – Mounting and Construction

To avoid issues pertaining to relative motions, the test apparatus was designed be mounted to a t-slotted experimental test bed. The spring mount was comprised of a plate that fastened to two t-slot nuts for connection to the test bed. The spring was fastened in the middle and bumpers were welded near its base to protect the spring from internal damage that could be inflicted from bottoming out due to overload. This fixture design is pictured below in Figure 4.

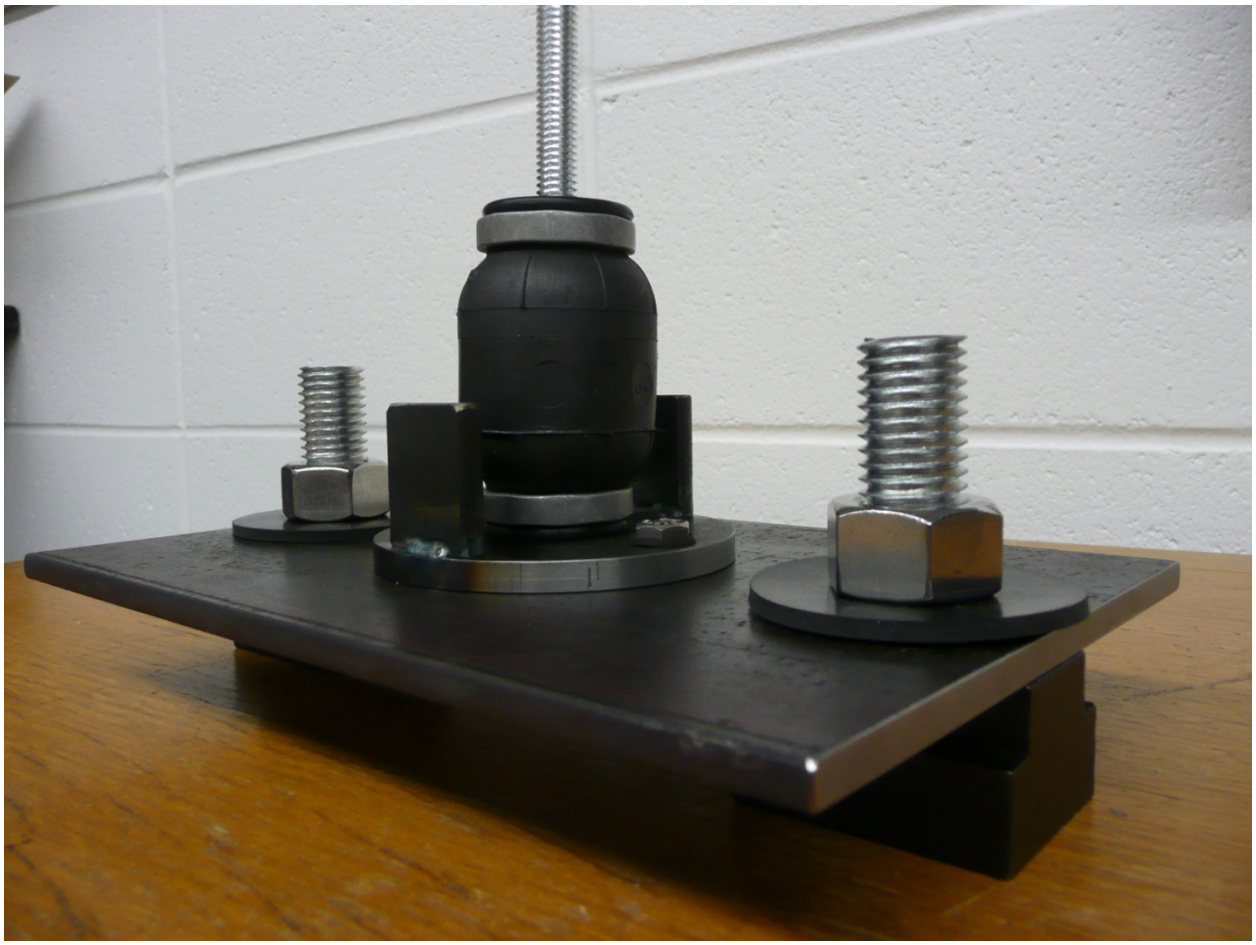

Figure 4 – Air spring mounting apparatus

After the springs were secured properly to the test bed, the beam was designed to be coupled to the springs at holes on each of its ends by a stud threaded to the top of each spring. For stability, the beam was designed to have an out-of-plane stiffness component via a steel wire fastened to the ground and around the body of the beam. These lateral beam supports provided stability through tension acting perpendicular to both sides of the beam in two places. This orientation effectively minimized any influence on motion or in-plane forces that are of interest, while providing necessary stability for proper functionality. The erected apparatus is displayed below in Figure 5.

Figure 5 – Fully-constructed experimental apparatus

4 - Experimentation

The dynamic parameters of the beam-air spring system were investigated by conducting testing in the frequency domain using an impulse test. The testing was performed to measure acceleration at various locations of the beam, as defined by the mode of linear displacement, in order to identify system parameters. After data collection, analysis was performed to supplement the results with theoretical comparisons.

With knowledge of acceleration data and control of the input force, it was possible to develop frequency response functions (FRF's) to analyze system behavior. The FRF methodology is a means to obtain the frequency response of the system by knowledge of time-domain data and implementation of digital Fourier Transform algorithms. Looking at equation (5), where an ideal impulse excitation has the value of a=1, the transfer function in the frequency domain is simply the output of the system. By considering the steady state time domain output acceleration and impulse excitation in the frequency domain, it is possible to define this magnitude response ratio, and equivalently, the system output. In this manner, the FRF of the system was defined as its accelerance. It was used to obtain the frequency response of the system by working in the imaginary plane:

$$FRF(j\omega) = \frac{FFT[a(t)]}{FFT[F(t)]} = \frac{a(j\omega)}{F(j\omega)} \qquad \frac{m/s^2}{N} \qquad (21)$$

The accelerance is a set of complex numbers that can be represented in the imaginary plane using polar notation. Accordingly, the complex number at each frequency will have a magnitude and angle. The magnitude ratio of the system can therefore be determined by taking the square root of the sum of the squares of the real and imaginary parts. It follows that the phase is just the angle between the real and imaginary parts. Doing this over a range of desired frequencies produces the frequency response of the system at each frequency in its domain. The spikes occurring in the magnitude response obtained through this methodology correspond to the location of resonant activity in the system, the natural frequencies of the system. These values are of primary importance in this design.

Figure 6 below displays the experimental setup for the impulse testing. A PCB impulse hammer, model 086C03, was used to excite the beam from its distal end at approximately 5/8" from the edge of the beam. A PCB 356A15 tri-axial accelerometer was used to measure the acceleration at locations defined as distal, center of gravity, and proximal (Figure 5). Acceleration data acquisition was performed using an HP 35670A dynamic signal analyzer. Five averages were performed on the acquired impulse data, using a frequency resolution of 1/32 Hz. By varying the locations of acceleration measurement as shown in Figure 7, it was possible to identify the mode shapes of the beam experimentally. In addition, the relationships between natural frequency, stiffness, damping ratio, and damping coefficient with respect to air spring pressure were investigated for both modes.

Figure 6 – Experimental setup for impulse testing of beam

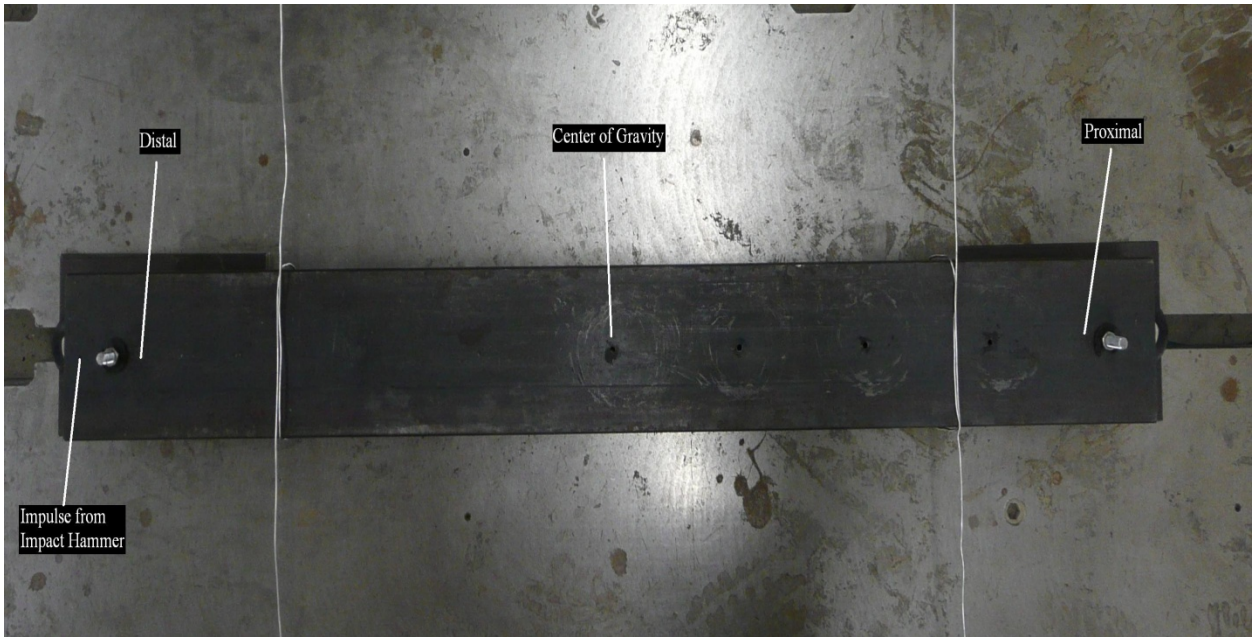

Figure 7 – Location conventions for impulse testing

The test matrix listed below in Table 1 lists the impulse trial procedure used to investigate the modal behavior. The pressure was regulated to each air spring at a constant 40, 60, or 80 psig. The accelerations were measured at the distal, center of gravity, and proximal locations for each pressure. This resulted in nine total trials conducted for the impulse test.

Table 1 – Test matrix for impulse testing of beam

Impulse Test - 2x Firestone 2M2A Air spring			
Pressure, (psig)	Accelerometer Location		
40	Distal	CG	Proximal
60	Distal	CG	Proximal
80	Distal	CG	Proximal

5 - Results

5.1 –Frequency Response and Natural Frequency Determination

Impulse testing was performed and experimental data was obtained over the frequency range of 0-50 Hz. In specific, coherence and frequency response data were obtained using the HP dynamic signal analyzer. The resulting data is summarized in Figures 8-16 below.

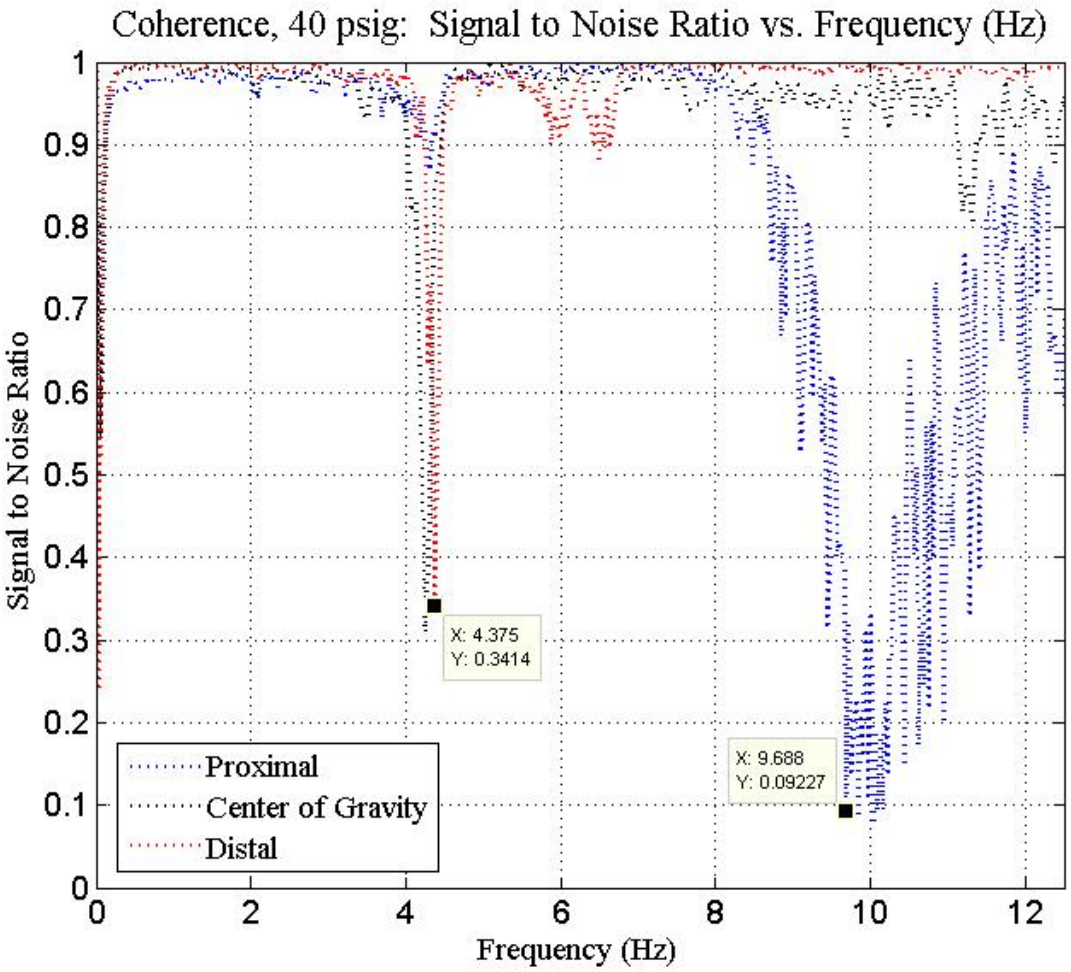

Figure 8 – Coherence of measurement system at 40 psig

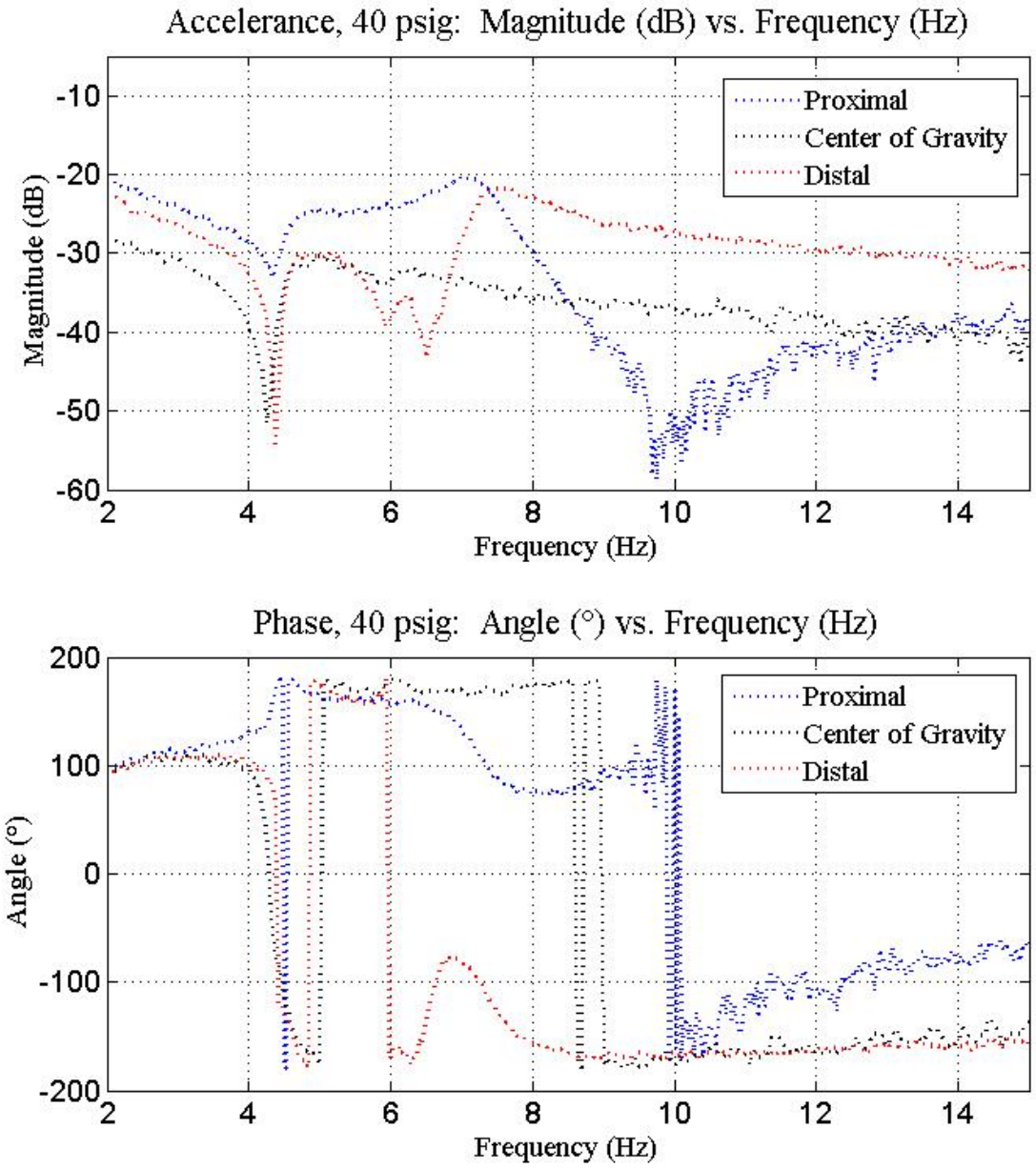

Figure 9 – Frequency response of beam at 40 psig

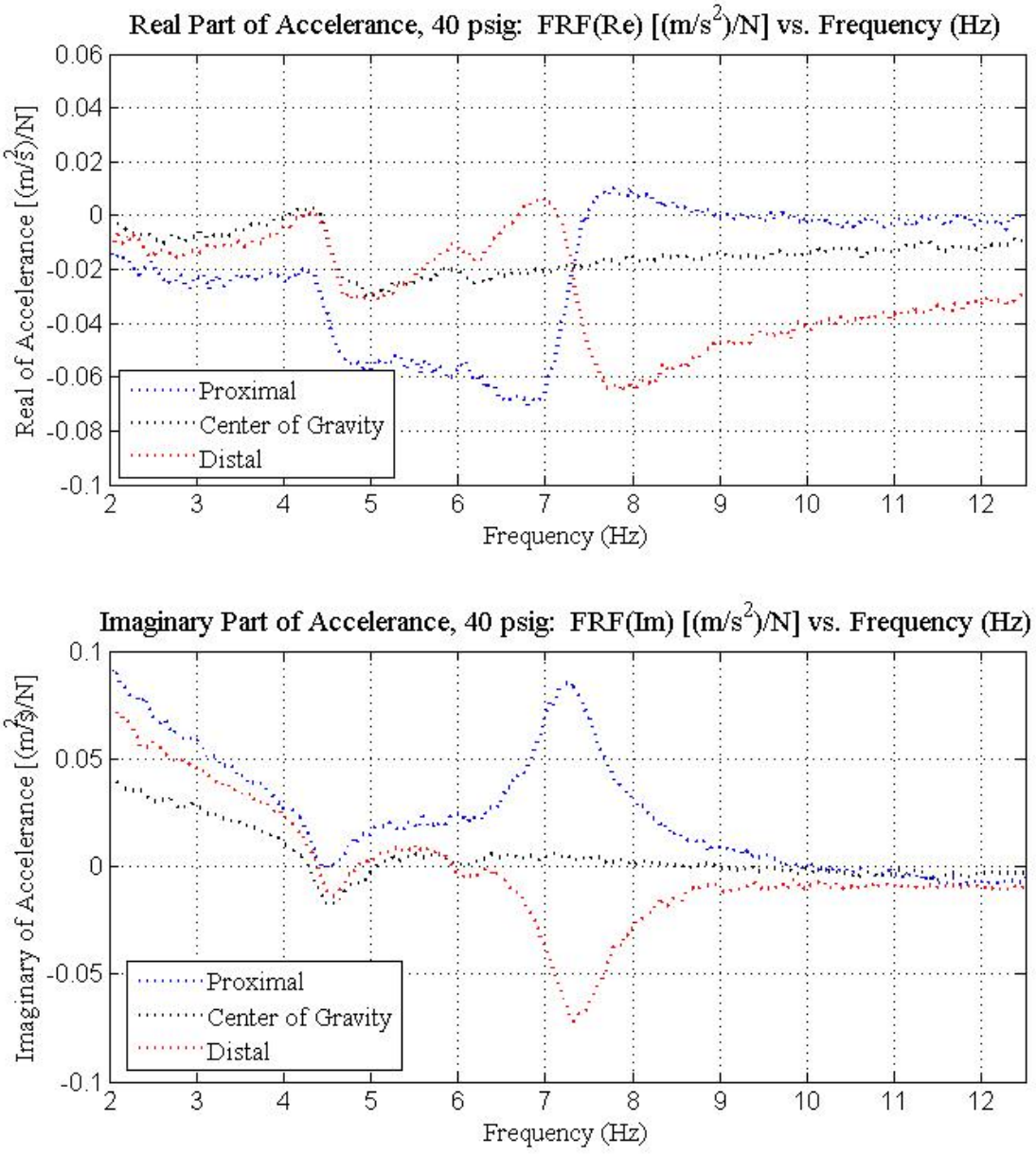

Figure 10 – Complex decomposition of accelerance at 40 psig

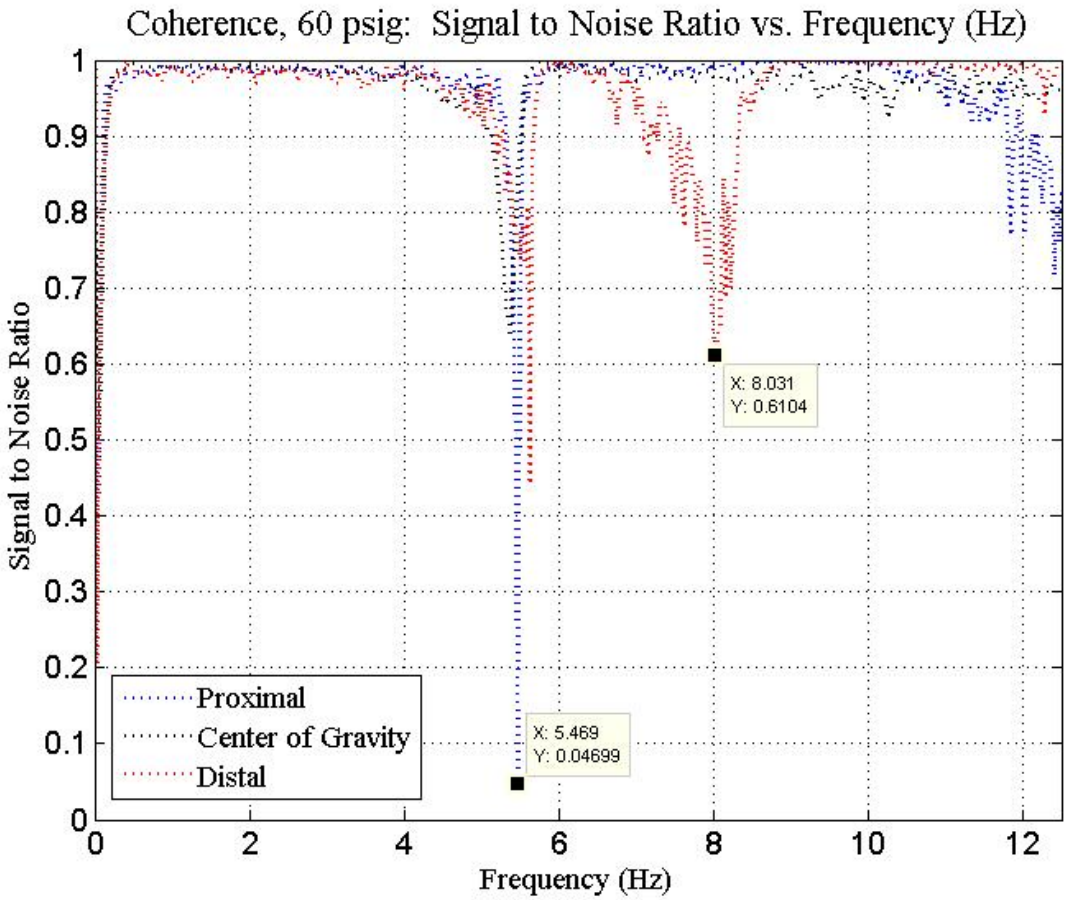

Figure 11 – Coherence of measurement system at 60 psig

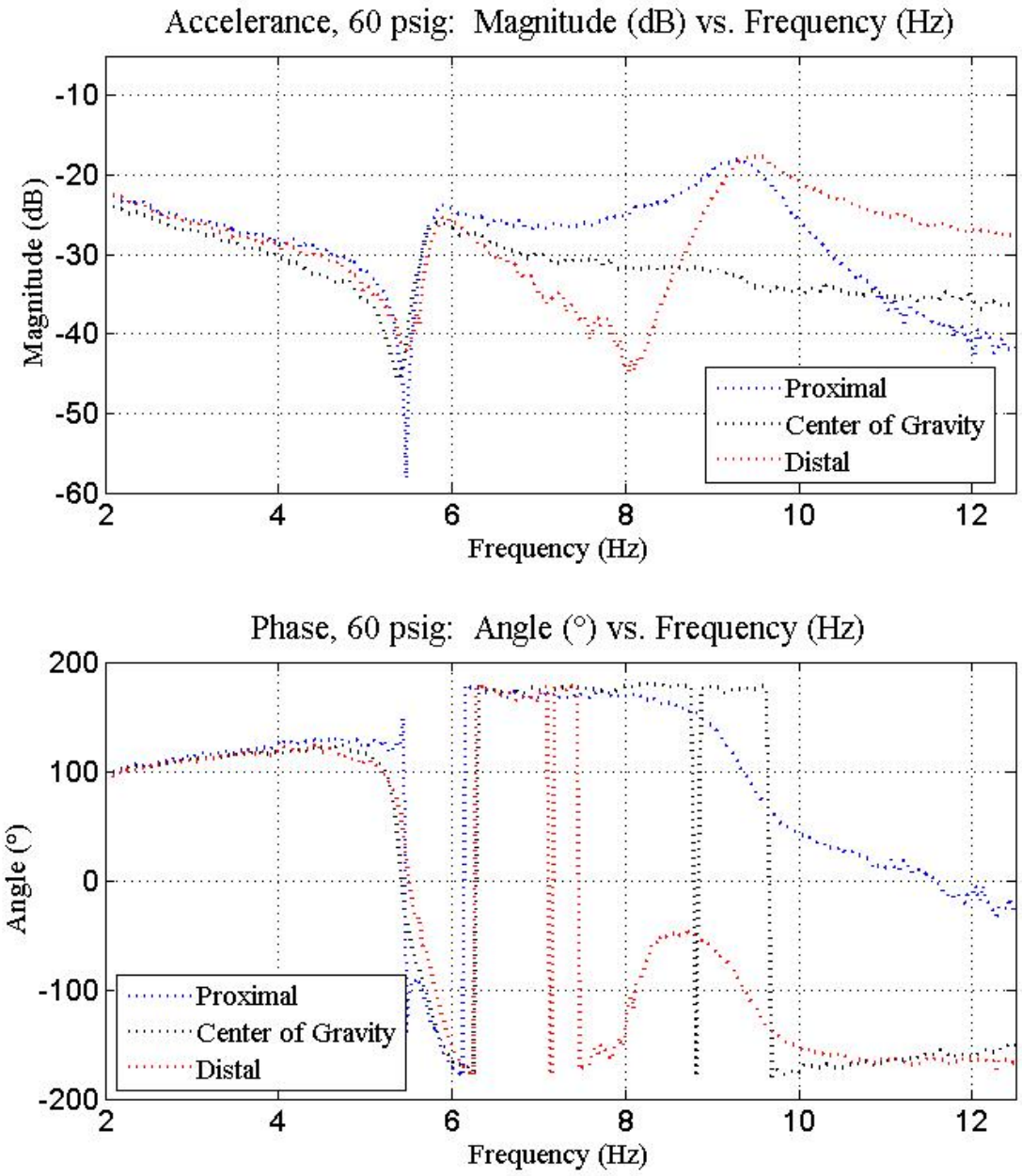

Figure 12 – Frequency response of beam at 60 psig

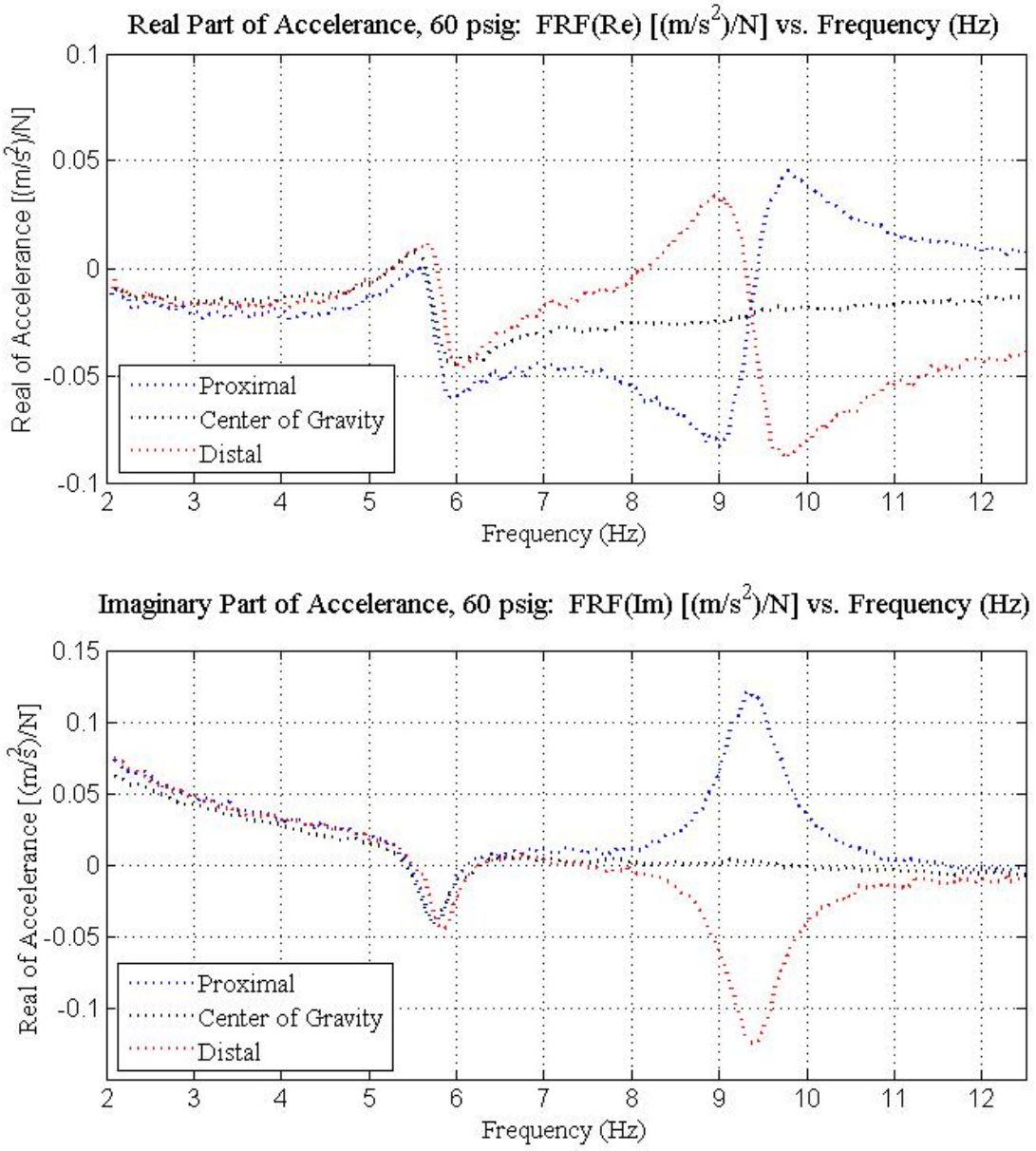

Figure 13 – Complex decomposition of accelerance at 60 psig

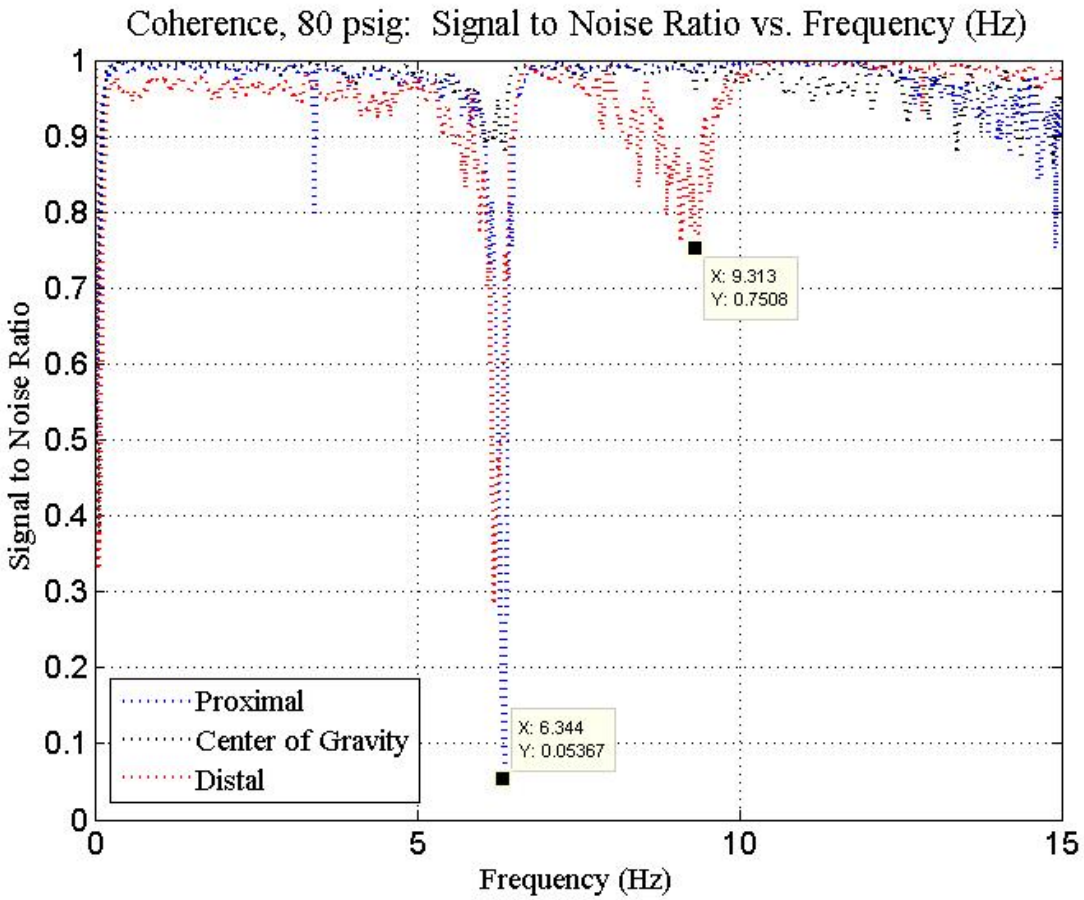

Figure 14 – Coherence of measurement system at 80 psig

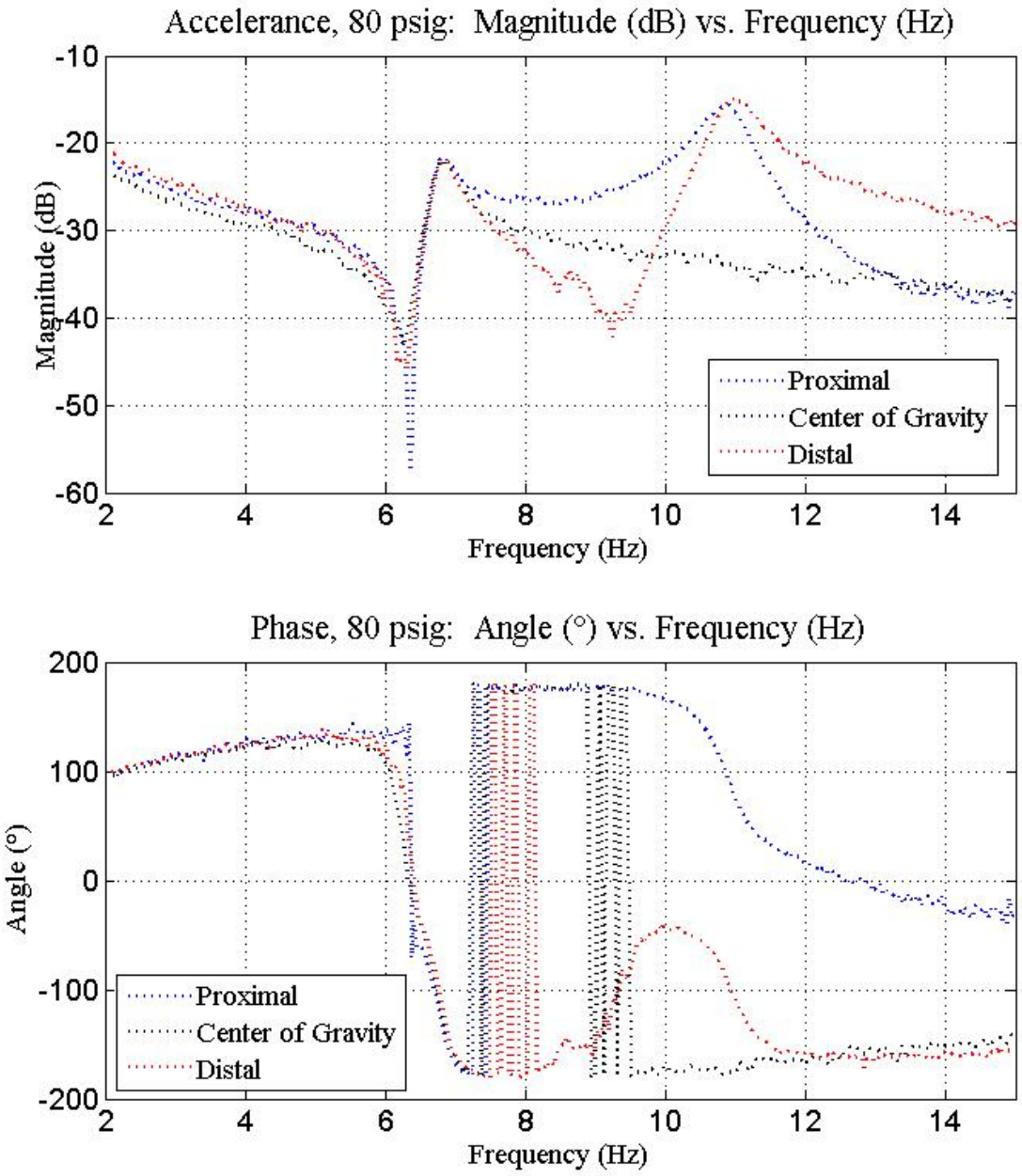

Figure 15 – Frequency response of beam at 80 psig

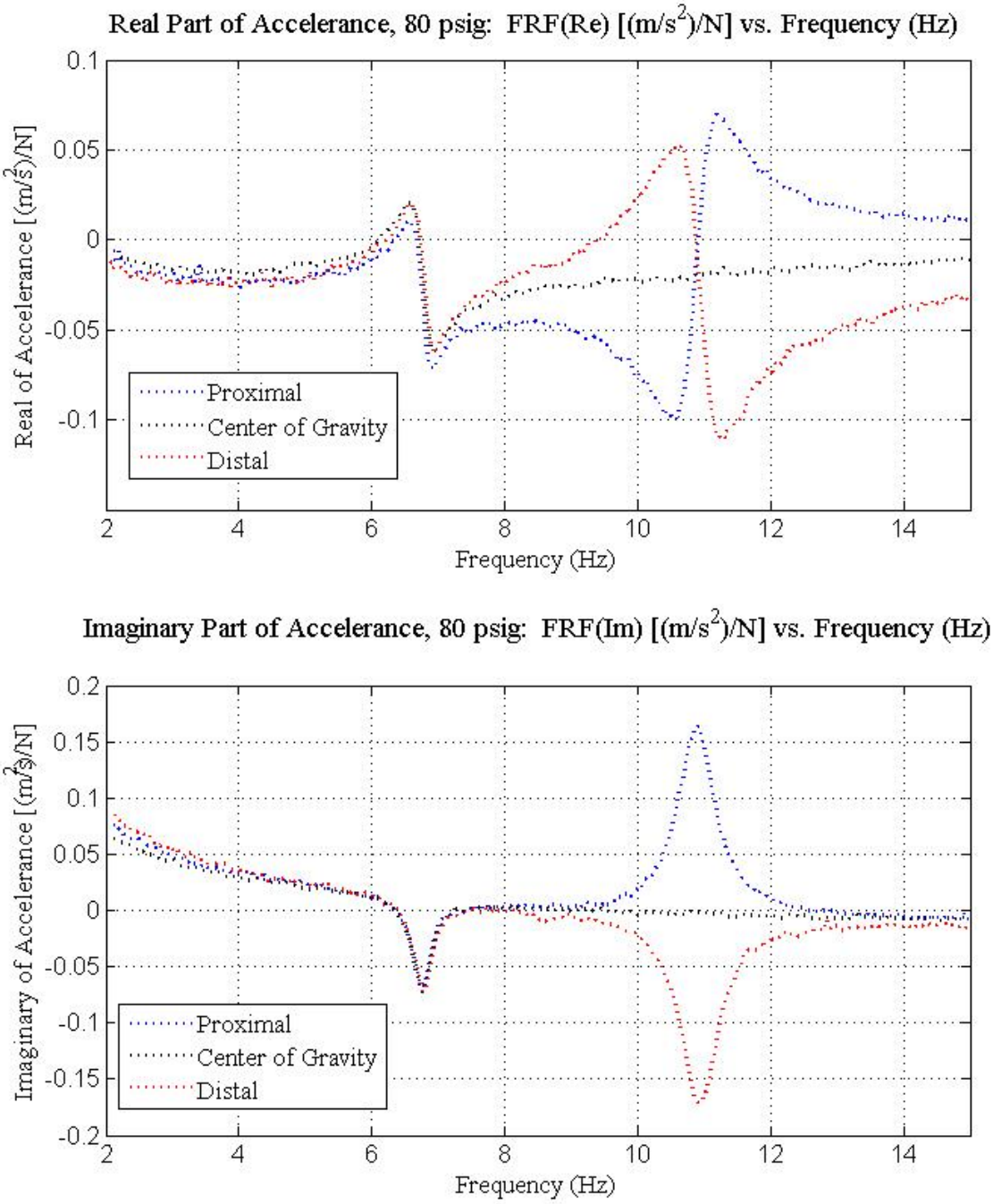

Figure 16 – Complex decomposition of accelerance at 80 psig

The experimental natural frequencies were determined by locating the frequency of the resonant peaks on the magnitude responses of Figures 9, 12, and 15. In addition, Figures 10, 13, and 16 displaying the complex decomposition of the accelerance were used to verify these natural frequencies. In particular, the natural frequency is defined as the location where the real of accelerance is exactly zero, which corresponds to the same frequency at which the peaks of the imaginary accelerance are located. It is worth noting that the real portion of the accelerance does always cross the frequency axis for both modes. This is not important, however, as elimination of systematic measurement system error would compensate for these offsets. The resulting experimental natural frequencies are displayed below in Table 2.

Table 2 – Summary of experimental natural frequencies by mode

System Natural Frequencies @ 40 psig					
	Proximal	CG	Distal	Modal Theory	% Difference
$\omega_{n,1}$ (Hz)	4.531	4.500	4.563	4.628	2.089
$\omega_{n,2}$ (Hz)	7.219	0.000	7.313	7.267	0.014
System Natural Frequencies @ 60 psig					
	Proximal	CG	Distal	Modal Theory	% Difference
$\omega_{n,1}$ (Hz)	5.719	5.750	5.844	5.953	3.057
$\omega_{n,2}$ (Hz)	9.313	0.000	9.375	9.347	0.032
System Natural Frequencies @ 80 psig					
	Proximal	CG	Distal	Modal Theory	% Difference
$\omega_{n,1}$ (Hz)	6.781	6.750	6.781	6.970	2.860
$\omega_{n,2}$ (Hz)	10.910	0.000	10.970	10.944	0.037

The experimental values of natural frequency presented in Table 2, which second as damped natural frequencies, have been compared to the undamped natural frequencies theoretically predicted using the eigenvector formulation for modal analysis (20). Since the natural frequency is a global parameter for a linear system, the eigenvalue problem was found to yield the same undamped natural frequency results for the system as defined by either (9) or (18), and for any and all values of d_1 and η. The amount of damping present in the system can be qualitatively assessed by observing the percent differences between these experimental and modal undamped natural frequencies. Accordingly, mode 1 displayed percent errors of 2.089-3.057% between the damped and undamped natural frequencies, whereas mode 2 tended to a 0% difference in damped and undamped natural frequencies with a range of 0.014-0.037%. Neither mode displays any significant difference in natural frequencies, therefore it follows that the damping is not expected to be substantial for either mode.

The plots of coherence in Figures 8, 11, and 14 accompanying the frequency response plot generated at each of the three air spring pressures can be used to assess the accuracy of the

frequency response measurement. Coherence is a quantity that can range in value from 0 to 1. It is based on the phase of the input and output signals for dynamic signal analyzers such as the HP35670A. In the case of this study, coherence was a measure of the percentage of power output by the accelerometer due to the power input by the impulse hammer trigger signal. Theoretically, when the coherence was a magnitude of 1, all the power from the accelerometer was due to the triggering event from the impact hammer. When coherence was 0, the accelerometer and impulse excitation from the hammer are completely random with respect to one another and therefore completely unrelated. For this reason, coherence can be used as a scale by which a measurement can be assessed for noise at a desired range of frequencies being investigated. The traditional signal-to-noise ratio used for coherence computations can be expressed as follows:

$$\frac{S}{N} = \frac{\gamma^2}{(1-\gamma)^2} \qquad (22)$$

A bad coherence is generally indicative of randomness and signal noise (from instrumentation or data acquisition), but has also been known to occur in the presence of system nonlinearities. From observation of the coherence plots for each air spring pressure setting, the coherence typically exhibited a trend of staying at or above 0.9 for frequencies under 10 Hz. Common to all coherence plots is a spike that occurred in the 4-6 Hz frequency range near the first mode, that of linear displacement. This spike sometimes approached coherence values of 0.1 or less, and was the reason for the anti-resonance value at the same frequency value in the corresponding magnitude response. This occurred in all instances, due to the fact that coherence is poor by definition at an anti-resonant frequency. Stated otherwise, no matter what the magnitude or type of excitation force, the acceleration will always be small at this frequency, therefore resulting in a small signal to noise ratio for the acceleration readings. For this reason, the coherence of 0.3414 at 4.375 Hz for the 40 psig configuration, 0.04699 at 5.469 Hz for the 60 psig configuration, and 0.05367 at 6.344 Hz for the 80 psig configuration will have no impact on the natural frequencies of the first mode. Poor coherence was also observed around 8.031 Hz and 9.313 Hz for the 60 psig and 80 psig scenarios, which are well below the experimental natural frequencies for the second mode. Lastly, poor coherence was encountered around 9.688 Hz for 40 psig, which is substantially higher in value than the natural frequencies for mode two here.

These exceptions to good coherence occurred at frequencies where the natural frequency was not observed in the magnitude response. In specific, the coherence at and around the natural frequencies for each pressure was observed to be around 1, which demonstrates the accuracy of the results.

5.2 – Analysis of System Mode Shapes

The mode shape of the system is the ratio that expresses the amount of relative motion between any two modes at a given resonant natural frequency. The mode shape is computed by manipulating the eigenvector from the eigenvalue problem for modal analysis, also called the modal vector. The modal vector takes the following form:

$$[v] = \begin{bmatrix} y_{1,\omega_{n,1}} & y_{1,\omega_{n,2}} \\ y_{x,\omega_{n,1}} & y_{x,\omega_{n,2}} \end{bmatrix} \qquad (23)$$

The mode shape is obtained by normalizing each column of the modal vector by the magnitude of its largest entry. Therefore, the mode shape will look like the following:

$$[m] = \begin{bmatrix} \frac{y_{1,\omega_{n,1}}}{y_{x,\omega_{n,1}}} & \frac{y_{1,\omega_{n,2}}}{y_{x,\omega_{n,2}}} \\ \frac{y_{x,\omega_{n,1}}}{y_{x,\omega_{n,1}}} & \frac{y_{x,\omega_{n,2}}}{y_{x,\omega_{n,2}}} \end{bmatrix} = \begin{bmatrix} \frac{y_{1,\omega_{n,1}}}{y_{x,\omega_{n,1}}} & \frac{y_{1,\omega_{n,2}}}{y_{x,\omega_{n,2}}} \\ 1 & 1 \end{bmatrix} \qquad (24)$$

Depending on the magnitudes of the entries in each column, it may be necessary to switch the order in which normalization is performed on the modal vector. From theory and (18), the entries in the modal vector can be manipulated for the desired locations along the span of the beam by specifying values for d_1 and η to match the experimental measurement locations. This will yield three different mode shapes: One which relates the motion of the proximal location to the center of gravity, one which relates the proximal and distal locations, and one that compares the center of gravity to distal location.

From experiment, the motion at three locations along the beam was measured. Although the real and imaginary parts of accelerance supplemented the determination of experimental natural frequencies, they are more useful in defining mode shapes for the system. Namely, the magnitudes of the imaginary portion of the accelerance can be used to define mode shape behavior between any two locations along the span of the beam by constructing an experimental modal vector. This can be performed as follows:

$$[v] = \begin{bmatrix} A_{1,\omega_{n,1}} & A_{1,\omega_{n,2}} \\ A_{2,\omega_{n,1}} & A_{2,\omega_{n,2}} \end{bmatrix};$$

$$[m] = \begin{bmatrix} \frac{A_{1,\omega_{n,1}}}{A_{2,\omega_{n,1}}} & \frac{A_{1,\omega_{n,2}}}{A_{2,\omega_{n,2}}} \\ \frac{A_{2,\omega_{n,1}}}{A_{2,\omega_{n,1}}} & \frac{A_{2,\omega_{n,2}}}{A_{2,\omega_{n,2}}} \end{bmatrix} = \begin{bmatrix} \frac{A_{1,\omega_{n,1}}}{A_{2,\omega_{n,1}}} & \frac{A_{1,\omega_{n,2}}}{A_{2,\omega_{n,2}}} \\ 1 & 1 \end{bmatrix} \qquad (25)$$

Note that $[m]$ is the normalized modal vector. Following this procedure, the theoretical and experimental mode shapes have been characterized in Table 3 below.

Table 3 – Comparison of theoretical and experimental modal vectors

Mode Shape Data @ 40 psig								
Location	Theory		Mode Shape		Exp		Mode Shape	
	$\omega_{n,1}$	$\omega_{n,2}$	$\omega_{n,1}$	$\omega_{n,2}$	$\omega_{n,1}$	$\omega_{n,2}$	$\omega_{n,1}$	$\omega_{n,2}$
Proximal	0.7071	1	1	1	-0.0004	0.08504	0.02351	1
CG	0.7071	-1E-06	1	-1E-06	-0.018	0.00509	1	0.05987
CG	-0.7071	-1E-06	1	1E-06	-0.018	0.00509	1	-0.0706
Distal	-0.7071	-1	1	1	-0.0142	-0.0721	0.78655	1
Proximal	-0.7071	-0.7071	1	1	-0.0004	0.08504	0.02989	1
Distal	-0.7071	0.7071	1	-1	-0.0142	-0.0721	1	-0.8474

Mode Shape Data @ 60 psig								
Location	Theory		Mode Shape		Exp		Mode Shape	
	$\omega_{n,1}$	$\omega_{n,2}$	$\omega_{n,1}$	$\omega_{n,2}$	$\omega_{n,1}$	$\omega_{n,2}$	$\omega_{n,1}$	$\omega_{n,2}$
Proximal	0.7071	1	1	1	-0.0407	0.1211	0.96792	1
CG	0.7071	1E-07	1	1E-07	-0.0421	0.00243	1	0.02005
CG	-0.7071	-1E-07	1	1E-07	-0.0421	0.00243	0.94413	-0.0195
Distal	-0.7071	-1	1	1	-0.0446	-0.1247	1	1
Proximal	-0.7071	0.7071	1	-1	-0.0407	0.1211	0.91384	-0.9711
Distal	-0.7071	-0.7071	1	1	-0.0446	-0.1247	1	1

Mode Shape Data @ 80 psig								
Location	Theory		Mode Shape		Exp		Mode Shape	
	$\omega_{n,1}$	$\omega_{n,2}$	$\omega_{n,1}$	$\omega_{n,2}$	$\omega_{n,1}$	$\omega_{n,2}$	$\omega_{n,1}$	$\omega_{n,2}$
Proximal	0.7071	1	1	1	-0.0665	0.1638	0.91527	1
CG	0.7071	-1E-07	1	-1E-07	-0.0727	-0.0016	1	-0.0095
CG	-0.7071	-1E-07	1	1E-07	-0.0727	-0.0016	0.99712	0.0091
Distal	-0.7071	-1	1	1	-0.0729	-0.1716	1	1
Proximal	-0.7071	0.7071	1	-1	-0.0665	0.1638	0.91263	-0.9545
Distal	-0.7071	-0.7071	1	1	-0.0729	-0.1716	1	1

Table 3 illustrates several trends about the system with respect to its two modes. These modes are normalized for better comparison in terms of [m]. Modes are also examined as the air spring pressure is varied. Overall, good agreement is seen between predicted and measured eigenvectors. For instance, the first eigenvector (primarily a translational mode shape) describes an in-phase motion and the system moves with almost unity (relative) amplitudes. The second

eigenvector (primarily a rotational mode shape) describes an out-of-phase motion and the system again moves with almost unity (relative, but opposite in sign) amplitudes.

5.3 –Modeling of Experiment

The design of this apparatus for low natural frequencies (large mass and low stiffness) has ultimately constrained the system. In specific, without large enough input force, finite displacement of the beam was not observed and subsequent nonlinear behavior could not be excited. This was the case for the low-magnitude excitation input from the impact hammer. As a result, the impulse test excited the beam system in a manner that was locally linear in behavior for all air spring pressures. For this reason, the dynamics of the system were well-approximated using linear transfer function theory.

Using (13) and (19), a transfer function model was derived to simulate the frequency response of the system at the proximal, center of gravity, and distal beam locations. To formulate an analytical linear model describing the motion of the beam, it was necessary to match the frequency response of the linear model to the experimental frequency response results by changing the stiffness and damping coefficients of the model. Changing the values of stiffness k_1 and k_2 were found to only alter the location of the model's resonant frequencies, while adjustment of the system's damping coefficients c_1 and c_2 only changed the values of the magnitude ratios. Accordingly, the stiffness was adjusted until the natural frequencies of the transfer function model best approximated the result found from impulse testing at the same location on the beam. Figure 17 displays the resulting natural frequencies of both modes as pressure was varied, and compares the results to experimental findings. For a given pressure and mode, the experimental natural frequency was taken to be the average value over all the locations of the beam. The system natural frequency and stiffness values for each pressure are also displayed in Tables 4 and 5.

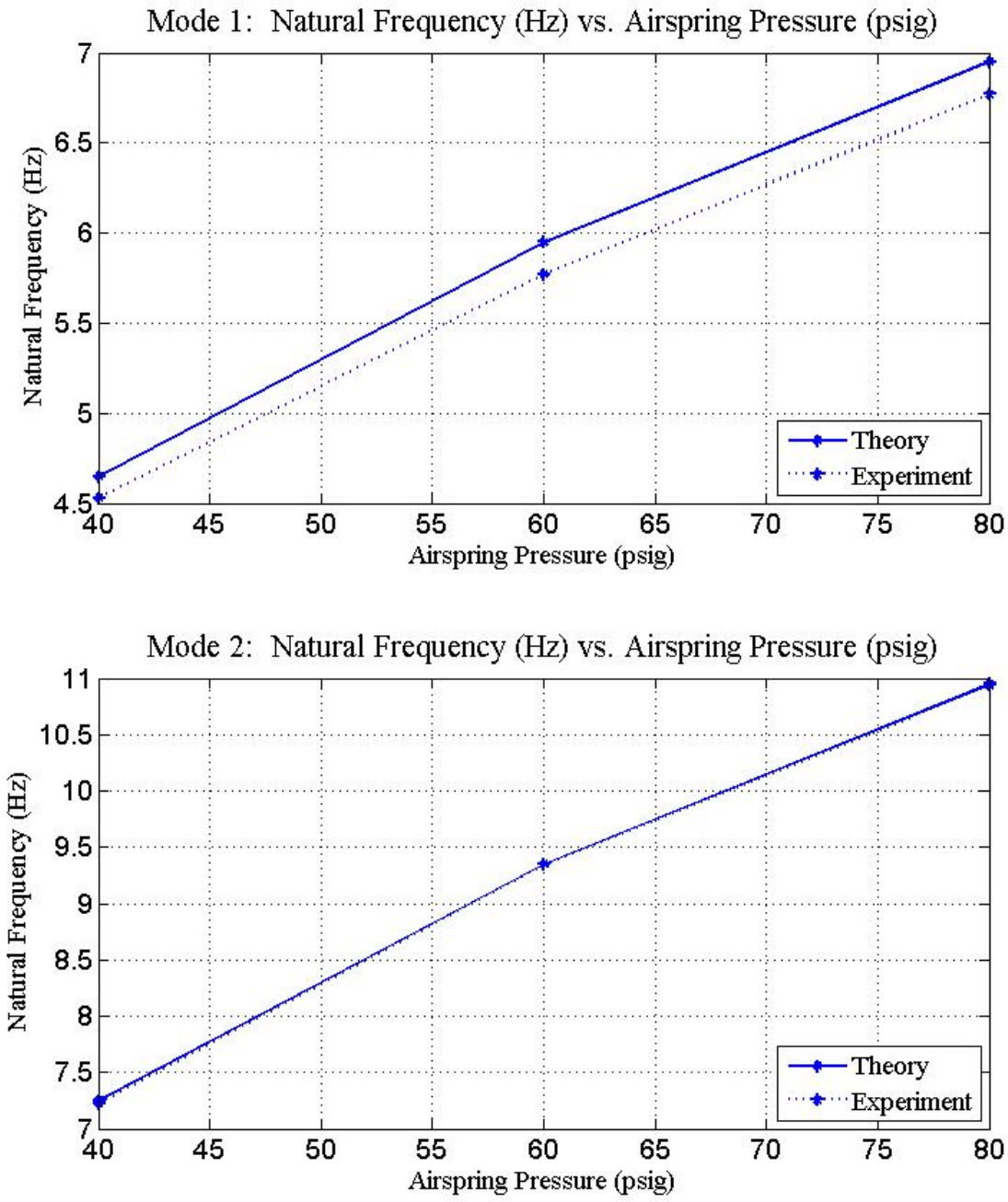

Figure 17 – Linear model vs. Experiment: Natural frequencies of system vs. air spring pressure

Table 4 – Linear model: Natural frequencies of system with respect to air spring pressures

Natural Frequencies		
Pressure (psig)	$\omega_{n,1}$ (Hz)	$\omega_{n,2}$ (Hz)
40	4.65	7.25
60	5.95	9.35
80	6.95	10.95

Table 5 – Linear model: Stiffnesses of system with respect to air spring pressures

Stiffness		
Pressure (psig)	K_1 (N/m)	K_2 (N/m)
40	23553.39	23553.39
60	38088.19	38088.19
80	53411.02	53411.02

From Figure 17, it can be seen that the values of air spring stiffness displayed in Table 4 yield a natural frequency solution that closely approximates the behavior of the experimental system over the range of tested pressures. Of special interest is the dynamic behavior of the system when the frequency response is taken at the center of gravity of the beam. In this situation, the natural frequency of the second mode does not appear in the frequency response of the system. This suggests that the system can be approximated as a one degree of freedom system when the mode corresponding to linear displacement is taken at the center of gravity. Intuitively, this also makes sense from a lumped-mass parameters standpoint, and is consistent with the dynamic coupling model of (7).

Instead of using iterative strategies, the linear approximation of system damping was accomplished through the application of previous results. When compared to the theoretical undamped natural frequencies listed in Table 2, the lower magnitude of the experimental natural frequencies reveal the underdamped condition of the system. For a second order system such as this, the damping ratios for the underdamped case can be found for any given pressure at each natural frequency using the following equations:

$$\zeta_{\omega_{n,1}} = \sqrt{1-\left(\frac{\overline{\omega_{d,1}}}{\omega_{n,1}}\right)^2}\,; \qquad \zeta_{\omega_{n,2}} = \sqrt{1-\left(\frac{\overline{\omega_{d,2}}}{\omega_{n,2}}\right)^2}\,; \tag{26}$$

In this case, $\omega_{n,1}$ and $\omega_{n,2}$ are the undamped natural frequencies from modal analysis. With knowledge of a modal vector and the undamped natural frequencies for that air spring pressure, it is possible to use the above calculated damping ratios to solve for values of the damping matrix of any coordinate system along the beam as so:

$$[C] = [\nu^T]^{-1} \begin{bmatrix} 2\zeta_{\omega_{n,1}}\omega_{n,1} & 0 \\ 0 & 2\zeta_{\omega_{n,2}}\omega_{n,2} \end{bmatrix} [\nu^T] \qquad (27)$$

Say the dynamics of the beam are described by the equations of motion in (18). It follows that:

$$[C] = \begin{pmatrix} c_1 + c_2 - \frac{c_2(L-d_1) - c_1 d_1}{\eta} & \frac{c_2(L-d_1) - c_1 d_1}{\eta} \\ c_2(L-d_1) - c_1 d_1 - \frac{c_1 d_1^{\,2} + c_2(L-d_1)^2}{\eta} & \frac{c_1 d_1^{\,2} + c_2(L-d_1)^2}{\eta} \end{pmatrix} \qquad (28)$$

Using the values along the main diagonal of [C], it is then possible to solve for unknown c_1 and c_2:

$$\begin{bmatrix} A & x \\ x & B \end{bmatrix} = \begin{pmatrix} c_1 + c_2 - \frac{c_2(L-d_1) - c_1 d_1}{\eta} & \frac{c_2(L-d_1) - c_1 d_1}{\eta} \\ c_2(L-d_1) - c_1 d_1 - \frac{c_1 d_1^{\,2} + c_2(L-d_1)^2}{\eta} & \frac{c_1 d_1^{\,2} + c_2(L-d_1)^2}{\eta} \end{pmatrix};$$

$$A = c_1 + c_2 - \frac{c_2(L-d_1) - c_1 d_1}{\eta}; \qquad (29)$$

$$B = \frac{c_1 d_1^{\,2} + c_2(L-d_1)^2}{\eta}$$

This technique was used to obtain the damping ratios and damping coefficients for each mode at all three pressures. Pictured below in Figure 18 is the resulting damping ratio of the system for both modes with respect to variation in the air spring pressure. Table 6 lists all of these values, in addition to the calculated damping coefficients for each pressure.

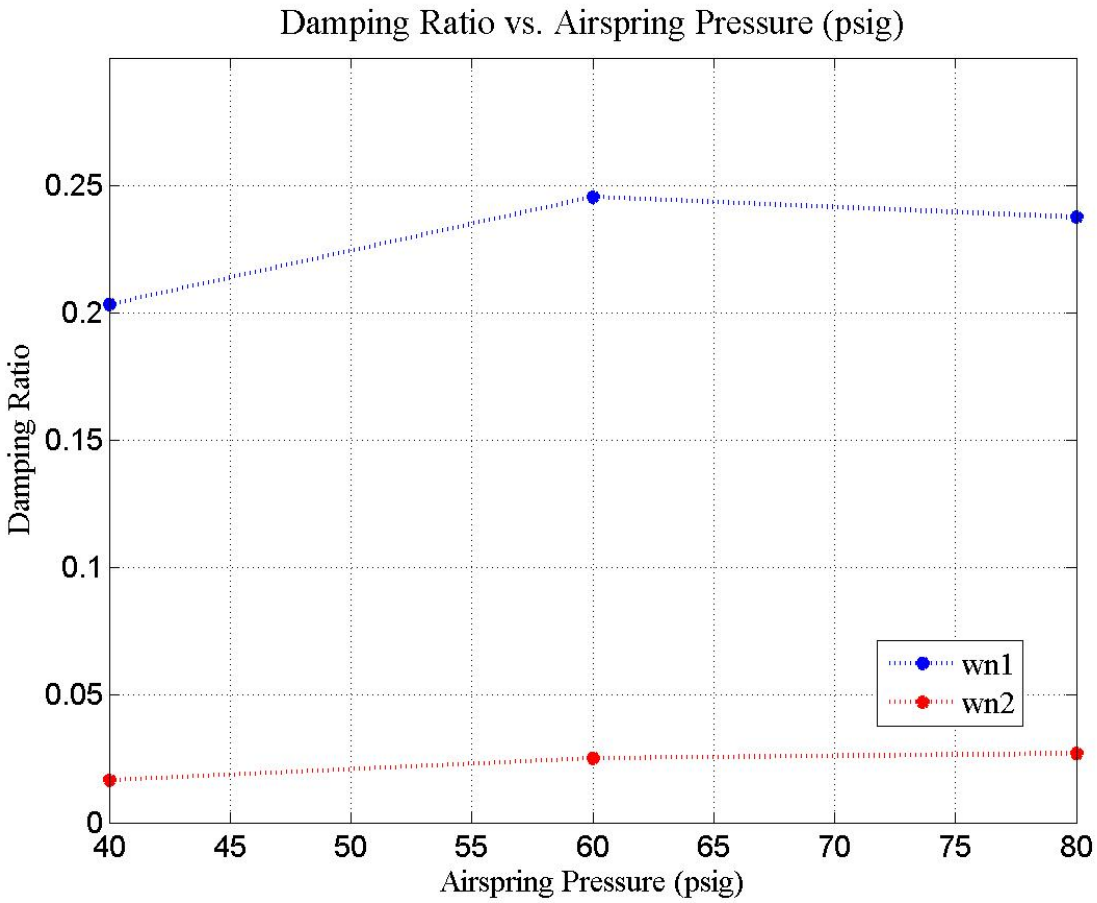

Figure 18 – Linear model: Damping ratio of system vs. air spring pressure

Table 6 – Linear model: Damping of system with respect to air spring pressures

	Damping			
Pressure (psig)	ζ @ $\omega_{n,1}$	ζ @ $\omega_{n,2}$	C_1 (N-s/m)	C_2 (N-s/m)
40	0.203319	0.01658909	12.127	0.7549
60	0.245379	0.02533405	19.1393	1.4846
80	0.237444	0.02703443	21.858	1.8557

The damping ratio of the system did not vary much as pressure was changed; however, the damping coefficients increased significantly with pressure. Of particular interest is the difference in damping coefficients c_1 and c_2. The damping coefficient located at the distal end of the beam exhibits a damping coefficient that is most likely attributed to the viscous damping introduced by the air springs, that which would normally not be found due to a typical structural spring element. However, the damping coefficient at the proximal end of the beam is substantially larger than expected, based on the damped natural frequency data obtained from experiment. These significant differences in damping can be attributed to the modes. System damping is significantly higher for either the displacement or rotational mode, although it cannot be determined which from this information alone.

Using the calculated stiffness and damping parameters for the linear model, the frequency response of the beam were created and are pictured in Figures 19-21.

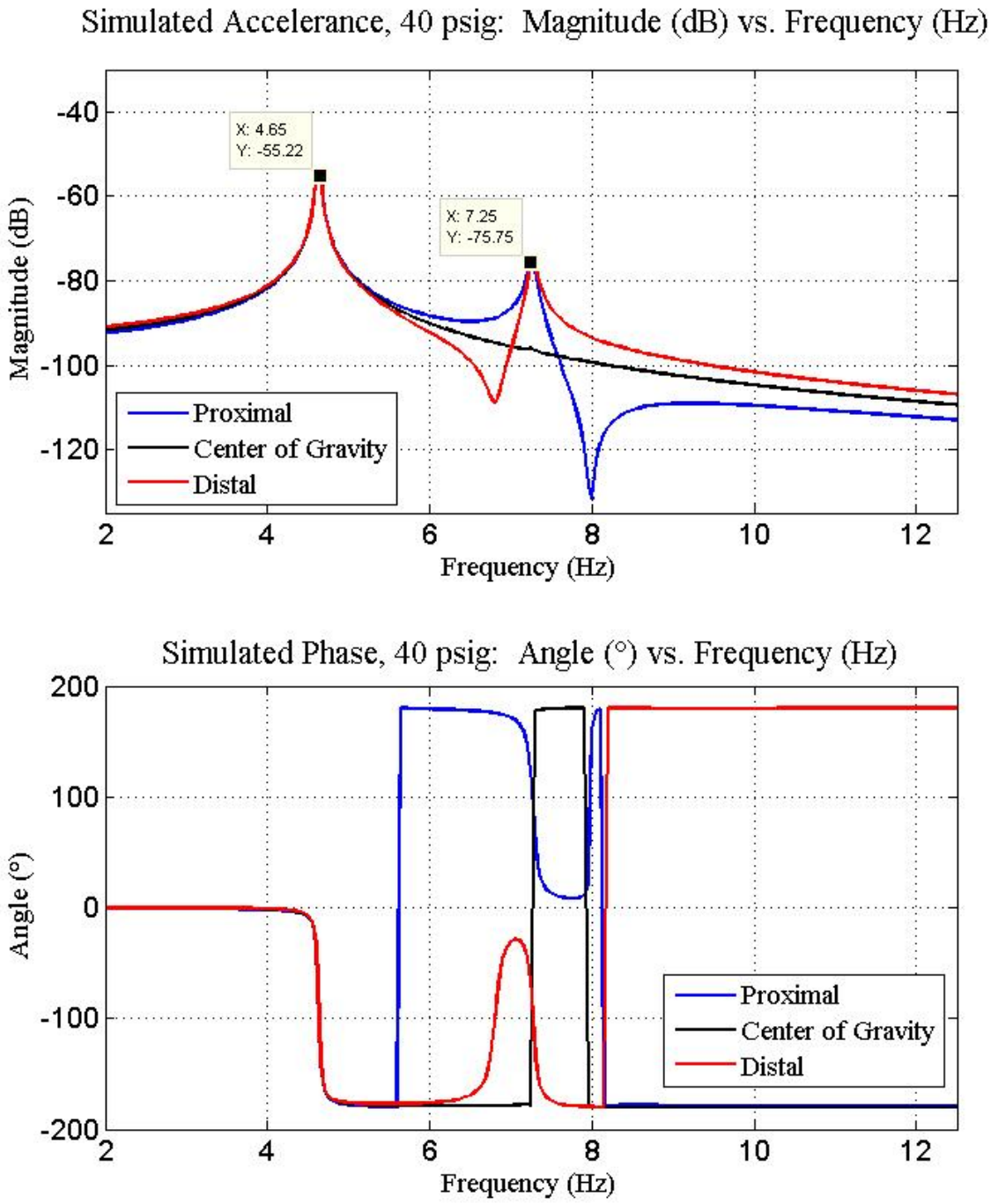

Figure 19 – Linear model: Frequency response of beam at 40 psig

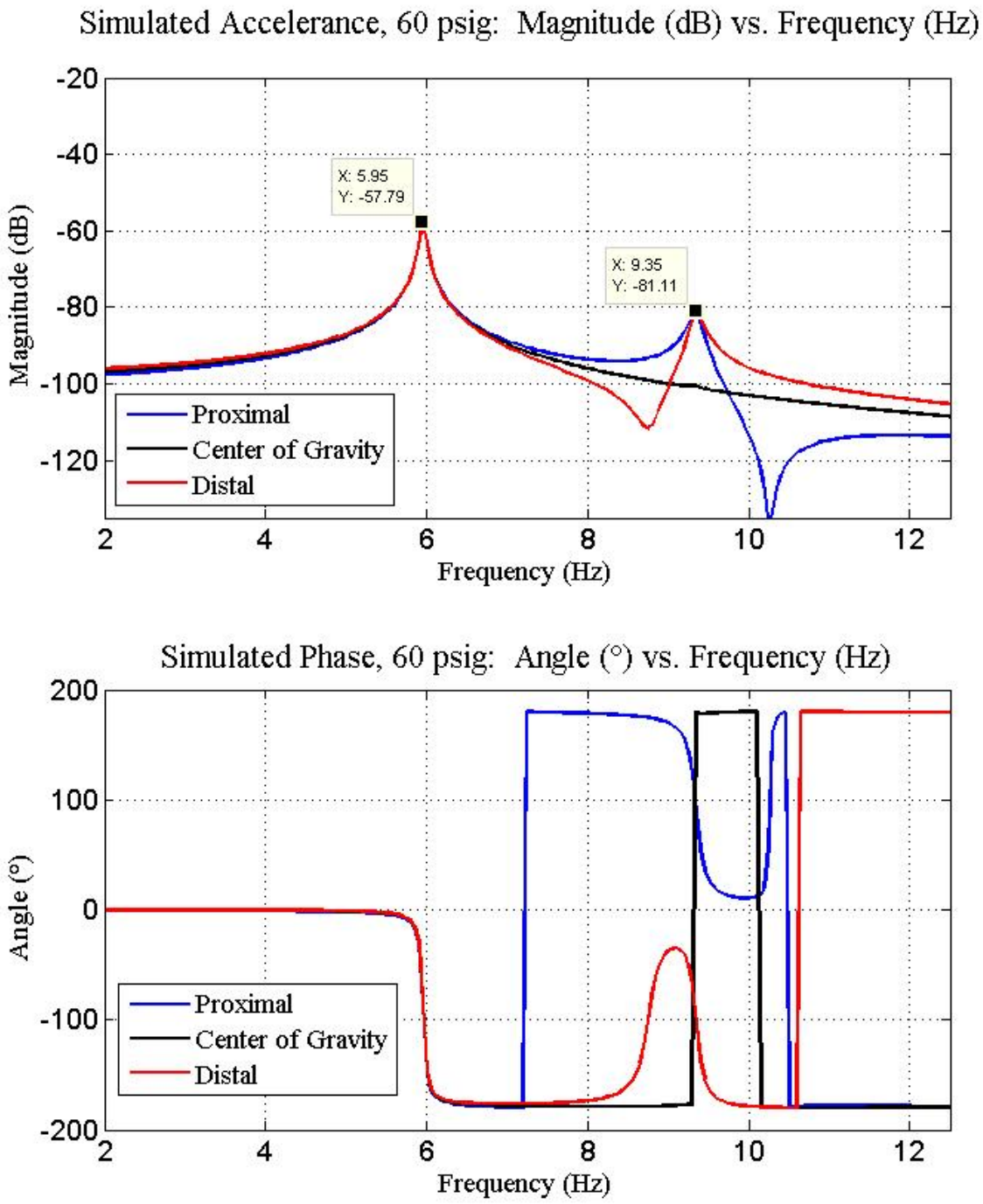

Figure 20 – Linear model: Frequency response of beam at 60 psig

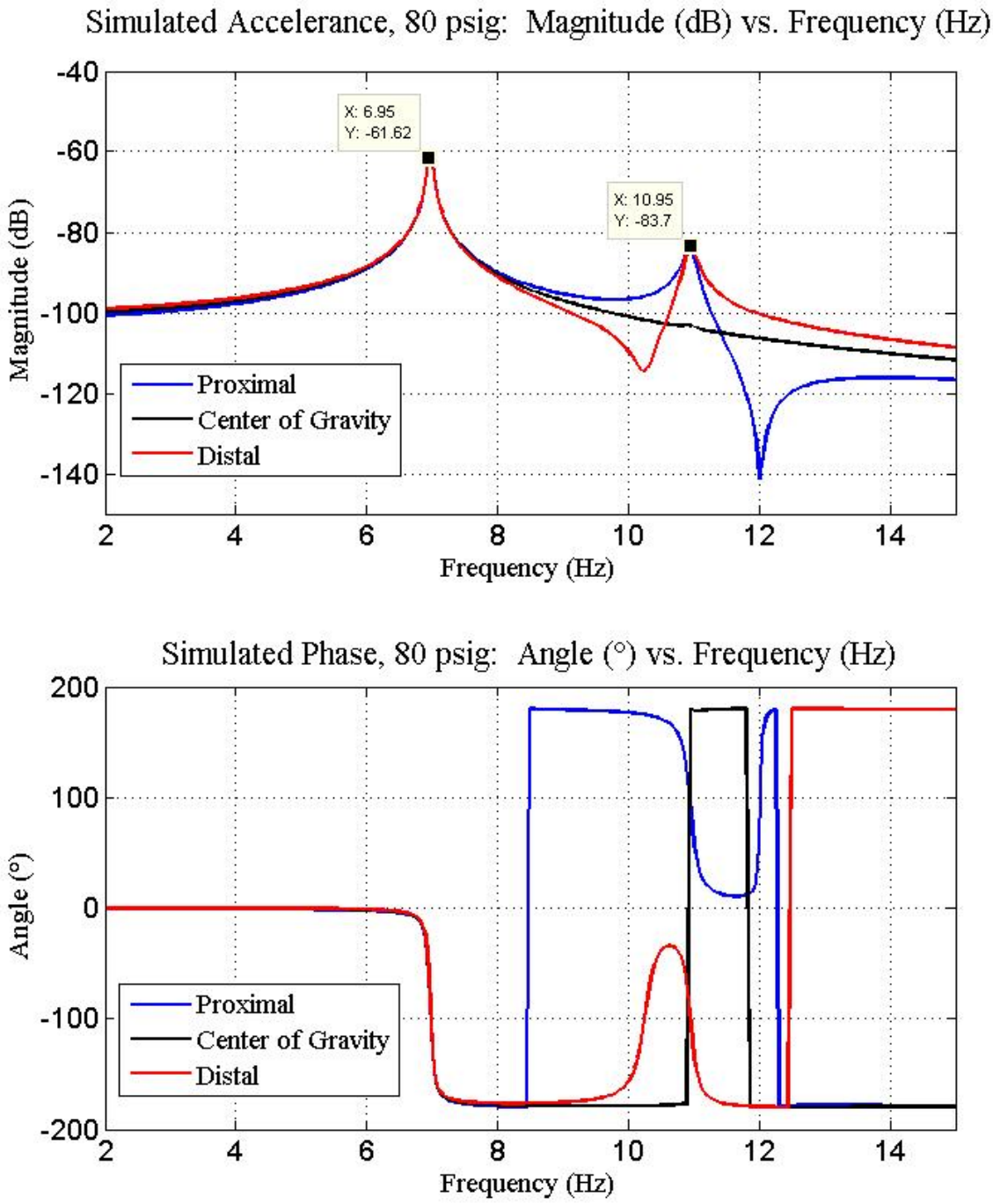

Figure 21 – Linear model: Frequency response of beam at 80 psig

When compared to the magnitude of the peaks corresponding to the experimental frequency response of the system, the linear model frequency response is substantially lower. This is due to the inexact nature of the natural frequency determination – that is, it was not possible to match both natural frequencies to the values displayed from experiment. By getting each natural frequency as close to the desired

experimentally observed value as possible, there was an inherent loss in magnitude due to the added distance from the expected resonant frequency. However, when the stiffness was adjusted to exactly match only one of the experimental natural frequencies, the magnitude of the natural frequency peak in the linear model very nearly approximated the dB level of that observed from experiment.

6 – Conclusions

The experiment was successfully designed and constructed to exhibit low frequency dynamics. In particular, this experiment simulates the dynamics of car suspension with success. Two natural frequencies are comparable to those encountered in a real-life car suspension system. The dynamics of the apparatus could be studied in a controlled manner. Further, the air spring stiffness elements (used to simply support the beam at its ends) are capable of introducing nonlinearities to the system under finite amplitudes.

An analytical model has been developed which successfully describes the dynamics of the beam-air spring setup. This linear model can be expressed in terms of translational and rotational displacements for pressures (at 40, 60, and 80 psig) as follows:

$$\begin{pmatrix} m & ml_g \\ ml_g & J \end{pmatrix}\begin{bmatrix} \frac{d^2y_1}{dt^2} \\ \frac{d^2\theta}{dt^2} \end{bmatrix}+\begin{pmatrix} c_1+c_2 & c_2(L-d_1)-c_1d_1 \\ c_2(L-d_1)-c_1d_1 & c_1d_1^{\,2}+c_2(L-d_1)^2 \end{pmatrix}\begin{bmatrix} \frac{dy_1}{dt} \\ \frac{d\theta}{dt} \end{bmatrix}+$$
$$\begin{pmatrix} k_1+k_2 & k_2(L-d_1)-k_1d_1 \\ k_2(L-d_1)-k_1d_1 & k_1d_1^{\,2}+k_2(L-d_1)^2 \end{pmatrix}\begin{bmatrix} y_1 \\ \theta \end{bmatrix}=\begin{bmatrix} aF(t) \\ s_1aF(t) \end{bmatrix}$$

OR

$$\begin{pmatrix} m-\frac{ml_g}{\eta} & \frac{ml_g}{\eta} \\ ml_g-\frac{J}{\eta} & \frac{J}{\eta} \end{pmatrix}\begin{bmatrix} \frac{d^2y_1}{dt^2} \\ \frac{d^2y_x}{dt^2} \end{bmatrix}+\begin{pmatrix} c_1+c_2-\frac{c_2(L-d_1)-c_1d_1}{\eta} & \frac{c_2(L-d_1)-c_1d_1}{\eta} \\ c_2(L-d_1)-c_1d_1-\frac{c_1d_1^{\,2}+c_2(L-d_1)^2}{\eta} & \frac{c_1d_1^{\,2}+c_2(L-d_1)^2}{\eta} \end{pmatrix}\begin{bmatrix} \frac{dy_1}{dt} \\ \frac{dy_x}{dt} \end{bmatrix}+$$
$$\begin{pmatrix} k_1+k_2-\frac{k_2(L-d_1)-k_1d_1}{\eta} & \frac{k_2(L-d_1)-k_1d_1}{\eta} \\ k_2(L-d_1)-k_1d_1-\frac{k_1d_1^{\,2}+k_2(L-d_1)^2}{\eta} & \frac{k_1d_1^{\,2}+k_2(L-d_1)^2}{\eta} \end{pmatrix}\begin{bmatrix} y_1 \\ y_x \end{bmatrix}=\begin{bmatrix} aF(t) \\ s_1aF(t) \end{bmatrix}$$

The analytical model has been shown to closely approximate the dynamic behavior of the beam in the frequency domain. This model is applicable for small displacements only and indeed the experiment has been shown to be linear. The stiffness, damping coefficients, natural frequencies and damping ratios of the system predict the behavior of the beam with success. However, no explanation for the damping coefficient behavior at the proximal end of the beam has been offered here.

By only performing an impulse test, nonlinear dynamics were not excited in the beam system during this study. It has been determined that a finite amplitude force would be required to observe large displacements due to the mass and size of the beam. For this reason, the type of nonlinearity (as exhibited by the air springs, for instance) could not be identified.

7 – Recommendations for Future Work

- Investigation of system damping
- Investigations of nonlinear dynamics (finite beam displacements)
    - Identify/define nonlinearity of the system
    - Enhance the nonlinearity by exciting it with finite amplitudes
    - Create of nonlinear models
    - Modify the experiment to illustrate clearance nonlinearities

Acknowledgements

Thank you to:

- My advisor, Dr. Singh, for all of your help and guidance
- Firestone, who helped sponsor this project by donating the air springs
- The Acoustics and Dynamics Lab and its members
- The Ohio State University Machine Shop
- Jerry Kingzett and the Ohio State Laboratory Staff

References

[1] Den Hartog, J.P., Mechanical Vibrations, Dover Publications, 1985.

[2] T.C. Kim, T.E. Rook and R. Singh, "Effect of Nonlinear Impact Damping on the Frequency Response Characteristics of a Torsional System with Clearance", Journal of Sound and Vibration, 281(3-5), 995-1021, 2005.

[3] Levy, Samuel and Wilkinson, John P.D., The Component Element Method in Dynamics, McGraw-Hill Book Company, 1976.

[4] C. Duan and R. Singh, "Dynamic Analysis of Preload Non-linearity in a Mechanical Oscillator", Journal of Sound and Vibration, 301, 963-979, 2007.

[5] Y. Yoshitake, A. Sueoka, "Forced self-excited vibration with dry friction", in: M. Wiercigroch, B. de Kraker (Eds.), Applied Nonlinear Dynamics and Chaos of Mechanical Systems with Discontinuities, World Scientific, Singapore, 2000 (Chapter 10).

[6] R.J. Rogers, P. Garland, M. Oliver, "Dynamic modeling of mechanical systems with opposing restraint preloaded stiffnesses", Journal of Sound and Vibration 274 (2004) 73–89.

[7] V.I. Babitsky, Theory of Vibro-Impact Systems and Applications, Springer, Berlin, 1998.

[8] Thomson, William T. Theory of Vibration with Applications. Englewood Cliffs, NJ: Prentice Hall, 1993. 138-45.